

Infrared properties of Planetary Nebulae with [WR] and *wels* central stars

C. Muthumariappan¹ * M. Parthasarathy^{1,2}

¹*Indian Institute of Astrophysics, Bangalore 560 034, India*

²*National Astronomical Observatory of Japan (NAOJ), 2-21-1 Osawa, Mitaka, Tokyo 181-8588, Japan*

Accepted ——. Received original form ——

ABSTRACT

We report the IR properties of planetary nebulae with WR type and *wels* central stars known to date and compare them with the IR properties of a sample of PNe with H-rich central stars. We use near-, mid- and far-IR photometric data from archives to derive the IR properties of PNe. We have constructed IR colour-colour diagrams of PNe using measurements from 2MASS, IRAS, WISE and Akari bands. [WR] PNe have a larger near-IR emission from the hot dust component and also show a tendency for stronger $12\mu\text{m}$ emission as compared to the other two groups. Cool AGB dust properties of all PNe are found to be similar. We derived the dust colour temperatures, dust masses, dust-to-gas mass ratios, IR luminosities and IR excess of PNe for these three groups. [WR] PNe and *wels*-PNe tend to have larger mean values for dust mass when compared to the third group. The average dust-to-gas mass ratio is found to be similar for the three groups of PNe. While there is a strong correlation of dust temperature and IR luminosity with the age for the three groups of PNe, the dust mass, dust-to-gas mass ratios and IR excess are found to be non-varying as the PNe evolve. [WR] PNe and *wels*-PNe show very similar distribution of excitation classes and also show similar distribution with Galactic latitude.

Key words: stars: AGB and post-AGB– nebulae : planetary — Stars : Circumstellar dust– stars: evolution

* E-mail: muthu@iiap.res.in

1 INTRODUCTION

The planetary nebula phase (PN, plural PNe) occurs in the evolution of low- and intermediate mass stars after the end of AGB phase and before the resulting white-dwarf configuration. Based on the surface composition, the central stars of PNe (CSPNe) are divided into two groups i.e. hydrogen-rich and hydrogen-deficient (Mendez 1991). The central stars of most PNe are in the first group (Todt, Grafener & Hamann 2006) which have thin hydrogen burning envelope and show hydrogen abundance close to the cosmic value on the surface (normal PNe, hereafter). About 30% of the CSPNe (Mendez 1991) belong to the second group where hydrogen is depleted in the stellar atmosphere and helium and carbon are the most abundant elements. From their spectral appearance one can distinguish between different types of hydrogen deficient CSPNe. A sizeable number of CSPNe (about 7%) are known to exhibit Wolf-Rayet type spectrum (hereafter [WR] stars; see Crowther 2008). [WR] stars have hydrogen deficient atmospheres and display broad emission lines of highly ionized carbon, oxygen and helium. They exhibit fast stellar winds (with terminal velocities up to 3000 km s^{-1}) with high mass-loss rates, up to two orders of magnitudes higher than the normal CSPN. Their spectra resemble the spectra of massive population I Wolf-Rayet stars of the carbon sequence. However, [WR] stars are low mass stars with degenerate structure. There is another group of CSPNe which show weak and narrow emission lines at the same wavelengths as those of [WR] stars which are called the weak emission lines stars (*wels*). However, unlike [WR] stars which are strictly hydrogen-deficient, the *wels* do not necessarily have hydrogen-deficient atmospheres, though many of them do (Hajduk, Zijlstra & Gesicki 2010). Weidmann, Mendez & Gamen (2015) find that at least 26% of *wels* are H-rich O stars. The PNe with [WR] stars ([WR] PNe) are stronger emitters in the *IRAS* $12\mu\text{m}$ band (Zijlstra 2001) compared to other PNe and also show the presence of PAH emission (Szczerba et al. 2001). Some hydrogen deficient stars also show dominant absorption lines like PG 1159–035.

The emission spectra of [WR] stars reflect physical processes which are different from other CSPNe. The WR-type emission lines of CSPN are interpreted as evidence of strong stellar winds. Detailed spectral analyses have shown that [WR] stars lose mass at a rate of $10^{-6} M_{\odot} \text{ yr}^{-1}$ (Leuenhagen, Hamann & Jeffrey (1996); De Marco et al. 1997). This is up to two orders of magnitude higher than the typical mass-loss rate of a CSPN having hydrogen-rich atmosphere. A quantitative classification of [WR] stars based on the strengths

of emission lines from ions with different ionization potential is related to the temperature evolution and can give the evolutionary connection between [WR] stars of different subtypes. Such quantitative classification schemes of [WR] stars currently in use were given by Crowther, De Marco & Barlow (1998, CDB98) and by Acker & Neiner (2003, AN03). CDB98 find a continuity in the [WR] classification scheme from [WC] to [WO] and suggest that the sequence is primarily due to excitation rather than abundance. All subtypes are seen in a sequence of decreasing stellar temperature from [WO1] \rightarrow [WO4] \rightarrow [WC4] \rightarrow [WC11]. AN03 conclude from this an evolution of stars from post-AGB \rightarrow [WC11] \rightarrow [WC4] - [WO4] \rightarrow [WO1]. Both CDB98 and AN03 find a sparsity of CSPNe in the [WC6-8] subclasses indicating a rapid evolution through this range or a different evolutionary path leading to two ionization sequences which is not yet understood. On the other hand, *wels* do not have such a classification scheme.

Though there are pronounced differences between the [WR] stars and the hydrogen rich CSPNe in their spectra and photospheric abundances etc., the PNe with [WR] stars have many properties which are very similar to those shown by the PNe with hydrogen-rich CSPNe. Particularly the similarities are seen in the elemental abundances, electron densities and temperatures and the morphologies of the PNe (Gorny & Stansika 1995, Gorny 2001). This indicates that the [WR] phenomenon does not preferentially occur for massive progenitors. One difference between them could be the turbulence in the nebula: most [WR] stars (also some *wels*) have PNe with more turbulence which is almost absent for PNe with hydrogen-rich CSPNe as shown by Gesicki et al. (2006). They also show that the mass-averaged expansion velocities of [WR] PNe are higher than that for the PNe around *wels* (*wels*-PNe) as well as the normal PNe. Higher expansion velocities for the [WR] PNe were also shown earlier by Tylenda & Gorny (1993).

The evolutionary path of low and intermediate mass stars which give birth to hydrogen-deficient [WR] stars and *wels*, and how and when it differs from the evolutionary path followed by hydrogen-rich CSPNe are not well understood. The observed differences of photospheric abundances of [WR] stars with the surface abundances of hydrogen-rich CSPNe show that [WR] stars have helium burning shells (Tylenda & Gorny 1993). [WR] stars are the observational testing for the He burning CSPN model. Hence, a process which can deplete hydrogen from the CSPNe and enrich their atmospheres with helium must play an important role. A process to deplete hydrogen in the stellar photosphere is the late or very late thermal pulse occurring after the star has left the AGB phase (born-again scenario; Werner & Herwig

2006). The born-again ejecta show high fraction of carbonaceous dust, which requires large amount of carbon and very efficient dust formation (Borkowski et al. 1994, Zijlstra 2001). However, the abundances of born-again ejecta in the PNe A30 (Kingsburgh & Barlow 1994) and A58 (Wesson et al. 2008) are oxygen and neon rich as expected from a nova-like ejection. Alternative theories were proposed on the origin of [WR] PNe, some of them were based on binary interaction (De Marco 2008). However, the close binary fraction of CSPNe observed for [WR] PNe could be much lower than that for the hydrogen-rich PNe (Miszalski et al. 2009). In order to find if there is an evolutionary connection between [WR] stars and *wels* and how they are different from the evolutionary path followed by the central stars of normal PNe, it is required to investigate in detail the gas and dust properties of PNe surrounding these stars. Parthasarathy et al (1998) found that the characteristics of the spectra of *wels* are very similar to that of [WC]-PG1159 and they suggested an evolutionary sequence of [WCL] \rightarrow [WCE] \rightarrow *wels* to PG 1159.

A comparative study between PNe with emission line central stars and PNe with hydrogen rich central stars was given earlier by Acker, Gorny & Cuisinier (1996). Gesicky et al. (2006) have studied the kinematics and photo-ionization of nebula around [WR] stars. The chemical composition and other properties of 30 [WR] PNe and 18 *wels*-PNe were studied and were compared to a sample of normal PNe by Girard, Koppen & Acker (2007). Gorny et al. (2001) analysed the IR properties of 49 [WR] PNe and addressed the dust content using near- and mid-IR photometric and spectroscopic observations gathered from the literature. More [WR] PNe and *wels*-PNe are known now and a few [WR] PNe have been reclassified. In this paper a uniform analysis of PNe surrounding [WR] and *wels* central stars known to date is provided and compared with the IR properties of PNe around non-emission line central stars in order to address if their evolution is connected. We have updated previous IR photometric studies with all [WR] PNe (99) known to date and derive the IR colour-colour diagrams of PNe and their nebular and dust properties. We also use *WISE* and *Akari* photometric observations in addition to *2MASS* and *IRAS* data. Far-IR *Akari* data are used to trace the coolest dust of these PNe. The excitation classes of these PNe were also derived and are used. We make similar studies for a sample of 67 PNe with *wels* central stars known to date and a sample of randomly selected 100 normal PNe. We constrain the properties of [WR] PNe, *wels*-PNe and normal PNe and compare them taking into account previous studies. Finally, we discuss the nature of these three groups of PNe and address if there are evolutionary connections between them.

2 OBSERVATIONAL DATA

All the data required for this study were taken from the literature. The near-IR fluxes were calculated from the magnitudes at respective wavelengths which were obtained from the *2MASS* archive (Cutri et al. 2003) archive. *IRAS* (Neugebauer 1984) fluxes at 12-, 25-, 60- and 100 μm and *WISE* (Wright et al. 2010; Cutri et al. 2012) fluxes at 3.4-, 4.6-, 12- and 22 μm were used to span the mid- and far-IR emission. In addition, we have used archived fluxes from *Akari* (Ishihara et al. 2010) at its 65-, 90-, 140- and 160- μm bands to trace the emission from cold dust down to $\sim 30\text{K}$. The *2MASS* and *Akari* data used for this study are available at the NASA/IPAC Infrared Science Archive¹. All archival data we have used for this study have uncertainty measurements.

Our sample of [WR] PNe and *wels*-PNe are from the catalogue of spectral classification of CSPNe given by Weidmann & Gamen (2011). We have taken the nebular $H\beta$ fluxes and electron densities from Stasinska & Szczerba (1999). Emission line fluxes of [OIII] and He II are obtained from Strasbourg-ESO Catalogue of Galactic Planetary Nebulae (Acker, Ochsenein, Stenholm et al. 1992). Distances to PNe in our sample are from Frew, Parker & Bojicic (2016; FPB16 hereafter) which were derived using H_α surface brightness of the nebula *vs* its radius relationship. Recently, the distances for a sample of 16 PNe were given by Schonberner et al. (2018) using nebular angular expansion, and 128 PNe were given by Stanghellini et al. (2019) using GAIA parallaxes measurements (second GAIA release). These authors have also compared their values with the distances given by FPB16 and have shown that they are in reasonably good agreement, though for a few cases the values differ. Moreover, FPB16 have the distance measurements for all candidates in our sample. We have also taken the $E(B - V)$ values of PNe from FPB16. Some objects do not have IR data in some bands and/or they do not have the nebular $H\beta$ flux and/or density and/or distance measurements.

3 IR COLOUR-COLOUR DIAGRAMS

IR colour-colour diagrams (CCDMs) are useful tools in studying the IR properties of celestial objects and are frequently being used by astronomers (Persi et al. 1987; Yerra et al. 2015). If the fluxes measured at two IR bands are f_{λ_1} and f_{λ_2} then the colour between the two

¹ <http://www.irsa.ipac.caltech.edu/applications/BabyGator/>

respective bands with central wavelengths λ_1 and λ_2 can be defined using the relation given by Plets et al. (1997):

$$c_{\lambda_1, \lambda_2} = 2.5 \times \log[(K_{\lambda_1}, z_{\lambda_1} f_{\lambda_2}) / (K_{\lambda_2}, z_{\lambda_2} f_{\lambda_1})] \quad (1)$$

where, K_{λ_1} and K_{λ_2} are the colour correction factors for the bands with central wavelengths λ_1 and λ_2 and z_1 and z_2 are their respective zero magnitude fluxes. For *IRAS* and *Akari* bands, where the measurements are given in fluxes, we have calculated the colours using this relation. For *2MASS* and *WISE* bands, where the measurements are in magnitudes, we have taken the difference of magnitudes at the two bands as the colour. The colour correction factors for *IRAS* photometry were taken from Neugebauer et al. (1984) corresponding to a power law spectral index of -1 and their zero magnitude fluxes are 28.3-, 6.73-, 1.19- and 0.43 Jy respectively at 12- 25-, 60- and 100 μ m bands (taken from [http : //www.ipac.caltech.edu/IRASdocs/exp.sub.ch6/C2a.html](http://www.ipac.caltech.edu/IRASdocs/exp.sub.ch6/C2a.html)). For the *Akari* bands, the colour correction factors for spectral index -1 at 65-, 90-, 140- and 160 μ m and the zero magnitude fluxes at these bands were taken from Shirahata et al. (2009). We have calculated the colours between two *IRAS* bands if the fluxes at these bands are given with uncertainty. The maximum error in the *IRAS* fluxes of our sample is 16%. Though there are many PNe which have *WISE* as well as *IRAS* measurements, some have either of that. In the following sections we discuss the CCDMs of near-IR, mid-IR and in far-IR bands for [WR] PNe, *wels*-PNe and normal PNe.

3.1 Near-IR colour analysis

Near-IR radiation from PNe consists of atomic emission lines and free-free and free-bound nebular continuum. In addition to this, hot dust present in the nebula also emits near-IR continuum and near-IR CCDM can bring out the dominant source of radiation at this wave band. We used the *2MASS* photometric measurements to calculate near-IR colours. Though some PNe in the sample have near-IR data from other sources, we have taken the *2MASS* data to be consistent and to make the study uniform with other PNe which have only *2MASS* data. The emission from PNe at this band can suffer significant extinction by interstellar dust on its way to the observer. Hence, interstellar reddening corrections were applied to the photometric measurements using the relations given by Whitelock (1985). The $E(B - V)$ values required for this correction were obtained from FPB16. We have made near-IR colour

analysis for 59 [WR] PNe, 42 *wels*-PNe and 63 normal PNe for which *2MASS* photometric measurements are available in the literature.

Fig 1 shows the extinction corrected colour-colour diagram of PNe plotted between $[J - H]$ and $[H - K]$ ($[J - H]_0$ and $[H - K]_0$) along with their errors. The errors in near-IR colours were calculated from the photometric errors in their respective bands obtained from archive and the error in $E(B - V)$ from FPB16. For reference we have also drawn a line in Fig 1 showing the stellar photospheric colours of main sequence stars (Koorneef 1983; S region); the bottom of the line represents the B-type stars and the top represents the M-type stars. Also shown in the figure is the nebular box (N region) which corresponds to the near-IR emission in the form of free-free, free-bound and ionic emission lines from the gaseous nebula (Whitelock 1985). A dashed line seen in Fig 1 represents the dust colours due to dust continuum emission (D region). This was computed with an emissivity exponent of 1 ($F_\nu = \nu B_\nu(T)$), which better represents the wavelength dependence continuum emission for circumstellar dust (Stasinska & Szczerba 1999; Muthumariappan, Kwok & Volk 2006). The bottom of this line corresponds to a dust colour temperature of 2000K and the temperature decreases along the line to 1000K at the top. Hence the location of a PN in this figure allows us to see the relative contribution from its different components (N, S or D) to the near-IR radiation.

Gorny et al. (2001) found from their near-IR CCDM that 9 [WR] PNe, which comprise about 30% of their [WR] PNe sample are located near the stellar main sequence line. They suggested that the similar colours to the main sequence stars imply that these PNe could have companion(s) to their [WR] central stars. It is also possible that the main sequence star may be a neighbouring star to the PN contaminating the near-IR flux. In our sample there are 8 [WR] PNe (PM 1-89 is not included here as it is identified as [WR] with a peculiar spectrum by Weidmann & Gamen 2011) which makes $\sim 14\%$ of our [WR] PNe sample. However, there are 12 candidates in the 'NS' region (see Fig 1a) where the contribution from both nebular and stellar components are important. Hence the [WR] PNe which have significant contribution from the main sequence stars becomes $\sim 34\%$ in our sample and is $\sim 43\%$ in the sample considered by Gorny et al. (2001). About 40% of [WR] PNe in the sample of Gorny et al. (2001) fall inside or around their nebular box, where the emission line of helium triplet at $1.083\mu\text{m}$ can be a major contributor (Whitelock 1985). However, our sample has only about 17% of [WR] PNe which are located inside or near to the nebular

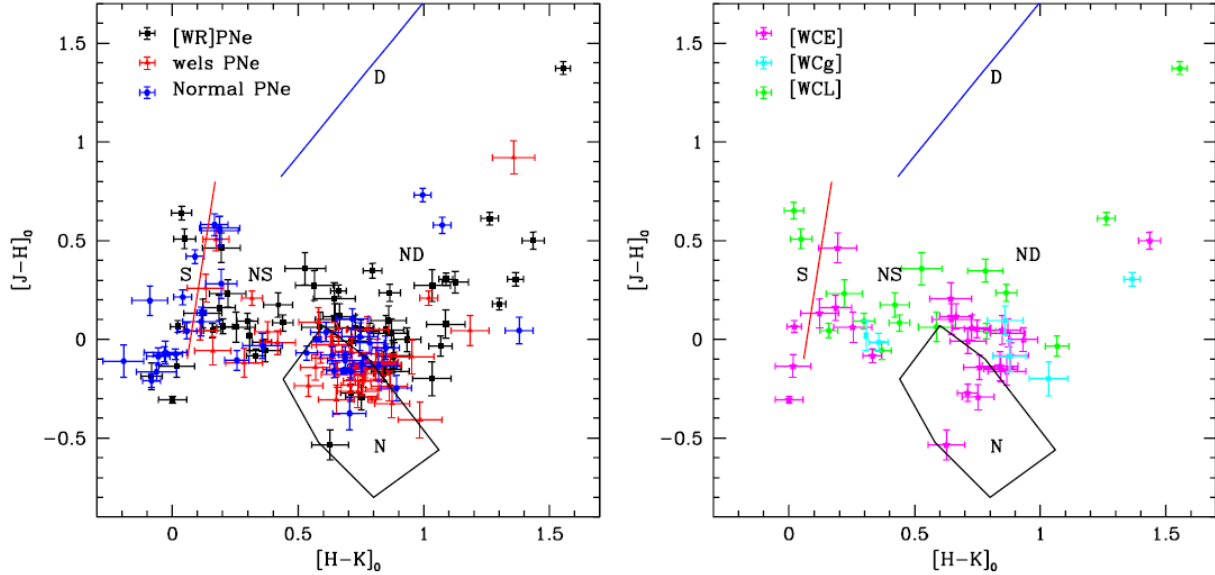


Figure 1. Extinction corrected near-IR colour-colour diagram of PNe using *2MASS* magnitudes. a) *Left:* for [WR] PNe, *wels*-PNe and normal PNe. *Right:* PNe with [WCL], [WCE] and intermediate type [WCg] central stars. The solid line 'S' in red is the stellar line, broken line 'D' in blue is the dust line and 'N' is the nebular box. See the text for details.

box. Hence most [WR] PNe are distributed away from the nebular box. In Fig 1a $\sim 42\%$ of [WR] PNe are located in the 'ND' region, where significant emission come from both the hot dust component and the nebular component. Fig 1b shows the near-IR CCDM for the subtypes of [WR] PNe, whose central stars were identified as late type, early type or intermediate type [WR] stars. The figure shows that there is no significant difference in the distribution of PNe with [WCL] and [WCE] stars in the 'NS' and 'ND' regions. Fig 1b also shows that none of the PNe with [WCL] stars are located inside the 'N' box, however, a few PNe with [WCE] stars are located inside 'N' box and some are seen closer to it. This could imply that more evolved [WR] PNe show brighter nebular emission.

As it is shown in Fig 1a, *wels*-PNe are concentrated in or close to the nebular box, in contrast to the [WR] PNe. Out of 42 *wels*-PNe, only 3 ($\sim 7\%$) are located near the stellar line and 5 ($\sim 12\%$) of them are seen in the 'NS' region. Their concentration in the 'ND' region is, however, significant (13, which is $\sim 31\%$). The near-IR colours of normal PNe are mostly distributed near the stellar line, inside or closer to the nebular box and in the 'NS' region. There are only a few of them located in the 'ND' region (10 out of 63 normal PNe in our sample; that is $\sim 16\%$). Those PNe falling close to the stellar line or in the 'NS' region of Fig 1a have the possibility of having binary nuclei, as suggested by Gorný et al (2001), which needs to be investigated.

Table 1. Mean values of colours between different IR bands and their dispersion for [WR] PNe, *wels*-PNe and normal PNe. The number of PNe in each class for which the colours were estimated are also shown.

Colour	[WR] PNe (No. of PNe)	<i>wels</i> -PNe (No. of PNe)	normal-PNe (No. of PNe)
<i>WISE</i>			
[3.4 – 4.2]	0.88±0.58 (63)	0.81±0.29 (47)	0.77±0.55 (72)
[4.2 – 12]	5.17±1.20 (63)	5.29±0.80 (47)	4.57±1.50 (71)
[12 – 22]	3.37±0.90(73)	3.65±0.55 (55)	3.65±1.10 (80)
<i>IRAS</i>			
[12 – 25]	3.45±0.63 (55)	3.95±0.50 (27)	3.73±0.70 (41)
[25 – 60]	2.41±0.74 (78)	2.38±0.54 (52)	2.38±0.86 (67)
[60 – 100]	0.21±0.50 (29)	0.17±0.65 (18)	0.68±0.54 (43)
<i>Akari</i>			
[65 – 90]	0.35±0.37 (50)	0.38±0.22 (35)	0.70±0.50 (53)
[90 – 140]	0.07±0.70 (45)	0.34±0.62 (26)	0.55±0.79 (48)
[140 – 160]	-0.11±1.10 (31)	-0.18±0.90 (19)	-0.46±1.20 (41)

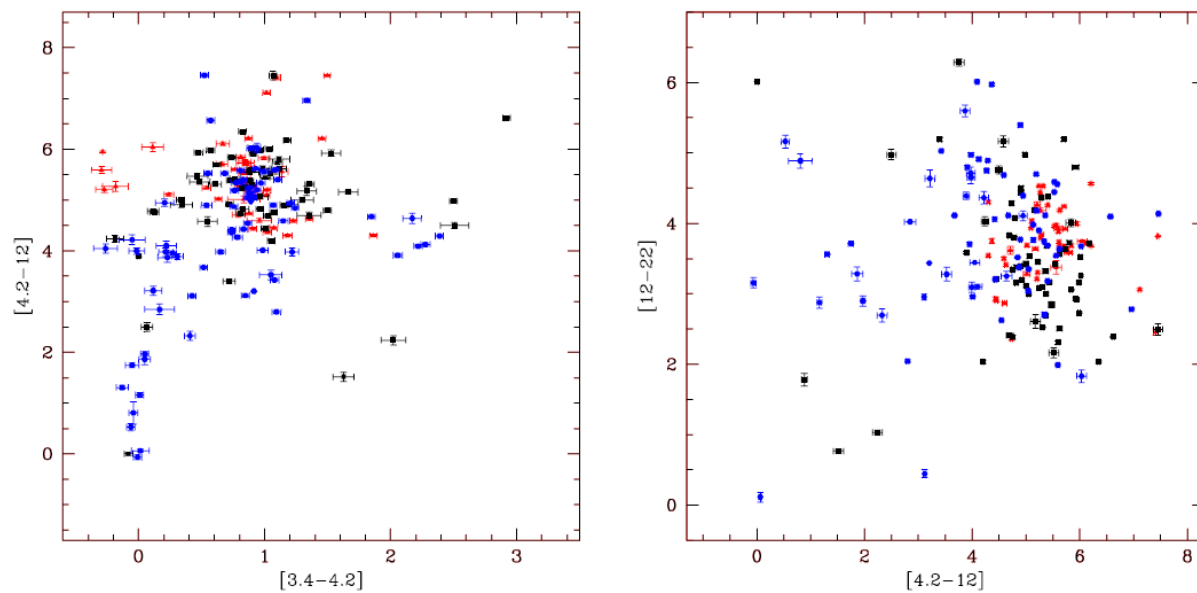


Figure 2. *WISE* colour-colour diagrams of PNe. Data description as given in Fig. 1. See the text for details.

3.2 Mid-IR colour analysis

Mid-IR radiation of PNe originate mostly from their warm, thermal equilibrium dust component which are at a typical colour temperature of $\sim 150\text{K} - 300\text{K}$. This dust was created in the cool and dense atmosphere of the AGB progenitor and is being heated by the hard UV radiation from the central star of the PN. The warm dust emission of a PN can be better traced by the N band ($10\mu\text{m}$) flux and also is seen in the Q band ($20\mu\text{m}$). In addition to this, the N band also includes the emission features of the Polycyclic Aromatic Hydrocarbons (PAH) and the atomic forbidden transitions. We construct the CCDMs using *WISE* bands at 3.6-, 4.5-, 12- and $22\mu\text{m}$ and *IRAS* bands at 12-, $25\mu\text{m}$ to study the properties

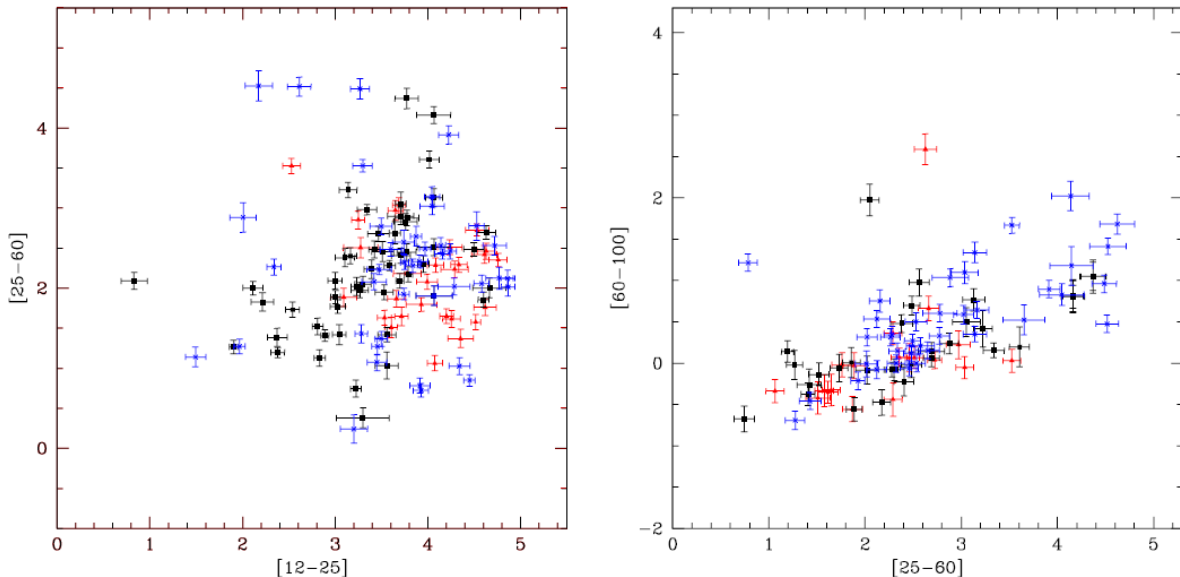


Figure 3. a (left) and b (right): *IRAS* colour-colour diagrams of [WR] PNe, *wels*-PNe and normal-PNe; data description as in Fig 1. See the text for details.

of hot and warm AGB dust. The $3.6\mu\text{m}$ and $4.5\mu\text{m}$ *WISE* bands respectively cover the PAH features at $3.3\mu\text{m}$ and $4.6\mu\text{m}$ and also have significant continuum emission from the hot dust component. The PAH features covered by the *WISE* $12\mu\text{m}$ band are at 7.7 -, 8.6 - and $11.3\mu\text{m}$ and by the *IRAS* $12\mu\text{m}$ band are at 8.6 - and $11.3\mu\text{m}$. In addition to the PAH features, the $12\mu\text{m}$ bands can also have atomic line fluxes of [Ar V] $7.9\mu\text{m}$ and [Ar IV] $9.0\mu\text{m}$, [S IV] $10.5\mu\text{m}$, [Ne II] $12.8\mu\text{m}$ and [Ne V] $14.3\mu\text{m}$. Relatively the $25\mu\text{m}$ band of *IRAS* and the $22\mu\text{m}$ band of *WISE* are least contaminated by atomic emission lines. Mid-IR CCDMs of PNe between these bands can be used to trace the relative emission contribution of the warm dust continuum, the PAH and atomic emissions in PNe. This can also bring out the differences in the emission components between [WR] PNe, *wels*-PNe and the normal-PNe. *WISE* colours are computed for these three groups of PNe, and are shown in Fig 2. Errors in the mid-IR colours are calculated from the errors in photometric measurements at their respective bands obtained from archive. Fig 3a shows the CCDMs of the three groups of PNe in the *IRAS* mid-IR bands. Table 4 shows the average values of mid-IR colours with their dispersions (or the range) of [WR] PNe, *wels*-PNe and normal-PNe.

Based on these colours we discuss the similarities and differences in the properties of warm AGB dust between these three groups of PNe. The mean values for *WISE* [3.3-4.6] and [4.6-12] colours of [WR] PNe are similar to those values derived for the other two groups of PNe, taking their dispersion into account. The mean values of *IRAS* [12-25] and *WISE*

[12-22] colours of *wels*-PNe are similar to their respective values of normal-PNe, however, [WR]PNe show somewhat lower values (see Table 1). Though the dispersions of mean values in *WISE* [12-22] colours are large, *IRAS* [12-25] colours show relatively smaller dispersions and indicates that [WR]PNe have a tendency towards a lower mean value than non-[WR] PNe. This also in turn indicates a possibility of a brighter $12\mu\text{m}$ band for [WR] PNe as compared to the other two groups. This was also suggested earlier by Zijlstra (2001) for a set of 40 [WR] PNe using *IRAS* data. Though the $12\mu\text{m}$ band is contaminated by atomic lines, the presence of strong PAH emission in this band can dominate over the atomic line fluxes, as discussed by Stasinska & Szczerba (1999) the emission from atomic lines become more important only for more evolved PNe. If we take that the contribution from atomic lines are not very important or that they are similar for all the three groups considered in this study, then the tendency for a brighter $12\mu\text{m}$ band shows that [WR] PNe likely to have stronger PAH emission as compared to *wels*-PNe and normal PNe. All the three CCDMs show that *wels*-PNe are least scattered in the mid-IR colour-colour plane. The *wels*-PNe are distributed with a spread which is $\sim 50\%$ lower than that for the normal-PNe, and the [WR] PNe are distributed similar to the normal PNe (see Fig 2 and Fig 3a). It shows that the mid-IR colours of *wels*-PNe group do not evolve that significantly as compared to that of the other two groups.

3.3 Far-IR colour analysis

The continuum emission from cool AGB dust in PNe (T_d less than 150K) can be best traced by the 25- and $60\mu\text{m}$ bands of *IRAS*, where the contamination due to dust features and atomic emission lines are minimal (Stasinska & Szczerba 1999). Also the dust continuum emission of PNe peaks in this wavelength domain. A study of this cool dust in [WR] PNe, *wels*-PNe and normal PNe will bring out the differences in their AGB evolution, if any. The mean values and dispersions of [25-60] colour for these three groups of PNe are calculated and are shown in Table 1 Also Fig 3a shows a plot of *IRAS* [12-25] *vs* [25-60] colours for them along with their errors. As can be seen in Table 1, the mean values of [25-60] colour for the three groups of PNe are nearly the same. The similarity in the [25-60] colour for [WR] PNe and non-[WR] PNe was also reported earlier by Zijlstra (2001). Our study hence supports the finding that the AGB dust properties inferred by [25-60] colours are similar for [WR] PNe, *wels*-PNe and normal PNe. Far-IR colours of the coolest dust in PNe are

studied using *IRAS* band at $100\mu\text{m}$ and *Akari* bands. Fig 3b shows the *IRAS* [25-60] vs [60-100] colours and *Akari* colours are plotted in Fig 4 along with their errors. As can be seen in Table 1, the mean values of *IRAS* [60-100] colour and *Akari* [65-90] colours are similar for [WR] PNe and *wels*-PNe taking their dispersion into account, but normal PNe have a tendency towards higher value (Table 1). Mean values of *Akari* [90-140] and [140-160] colours are also shown in Table 1.

In Fig 5 we show the Galactic distribution of [WR] PNe, *wels*-PNe and normal PNe at different latitudes. To see if their distributions are similar, we have performed a two sample Kolmogorov-Smirnov test between these groups of PNe. The value of the test statistics between the distributions of [WR] PNe and *wels*-PNe is $D = 0.017$ and the probability to find the test statistics below the critical value is $P = 0.99$. This shows that these two distributions are similar. However, the test performed between the distributions of [WR] PNe and normal PNe shows $D = 0.138$, $P = 0.63$ and between the distributions of *wels*-PNe against normal PNe shows the values of $D = 0.127$, $P = 0.58$. This brings out that the distribution of normal-PNe with Galactic latitude is somewhat different from that of [WR] PNe and of *wels*-PNe. [WR] PNe and *wels*-PNe are concentrated near the Galactic plane, however, normal PNe are commonly seen at higher latitudes. This is in contrast with the suggestion given by Acker, Gorny & Cuisinier (1996).

Table 2. Nebular parameters derived for [WR] PNe (see the text for details)

PNG	class	T_d (K)	M_d ($10^{-4}M_{\odot}$)	m_d/m_g (10^{-3})	L_{IR} (L_{\odot})	IRE	Exc. class
000.4-01.9	[WC5-6]	85	1.52±0.73	4.20±0.73	535±251	1.55±0.22	2
001.2-05.6	[WO1-2]	76	1.00±0.41	–	201±80	–	–
001.5-06.7	[WC9]pec	170	0.52±0.32	–	5825±2830	15.15±2.12	8
001.7-04.4	[WC11]	73	5.42±2.47	–	890±436	–	1
002.2-09.4	[WO4]pec	92	1.75±0.73	6.02±1.0	914±368	3.75±0.53	1
002.4-03.7	[WC11]	105	1.38±0.62	11.1±2.1	1392±612	5.23±0.74	–
002.4+05.8	[WO3]	85	0.85±0.37	3.12±0.6	300±131	1.23±0.17	5
002.6+05.5 ¹	[WC4]	–	–	–	–	–	11
003.1+02.9	[WO3]	81	1.89±0.82	4.95±0.86	522±221	1.73±0.24	7
004.8-22.7	[WC4]	115	1.84±0.75	–	2934±1250	–	–
004.9+04.9	[WC5-6]	90	2.13±1.0	6.0±1.0	997±478	2.53±0.36	2
005.9-02.6	[WC8]	–	–	–	–	–	–
006.0-03.6	[WC4]	86	1.73±0.72	2.9±0.5	642±340	1.63±0.23	3
006.8+04.1	[WC4]	89	2.01±0.89	2.6±0.45	888±385	1.67±0.24	6
007.8-03.7	[WC]	–	–	–	–	–	9
009.8-04.6	[WO2]	84	0.61±0.39	1.1±0.22	202±110	2.69±0.70	10
011.1-07.9	[WC12]	99	1.40±0.62	–	–	1055±447	–
011.9+04.2	[WO4]pec	94	1.60±0.57	2.13±0.5	929±418	5.52±0.75	–
012.2+04.9	[WC10]	99	4.30±1.9	–	3239±1458	–	–
016.8-01.7	[WR]	77	–	–	–	–	–
017.9-04.8	[WO2]	77	0.67±0.35	8.7±1.5	145±64	1.74±0.25	11
019.7-04.5	[WC4]	87	3.41±0.55	4.9±0.6	1348±741	2.80±0.74	3
020.9-01.1	[WO4]pec	90	1.33±0.63	2.5±0.47	625±287	1.80±0.25	2
021.0-04.1	[WC4]	–	–	–	–	–	–
027.6+04.2	[WC7-8]	140	2.23±1.1	3.2±0.55	9499±4788	7.50±1.06	2
029.0+00.4	WC	–	–	–	–	–	1
029.2-05.9	[WO4]	91	1.1±0.47	5.7±0.98	547±226	6.8±0.96	3
037.5-05.1	[WCE]	89	10.80±5.3	–	4782±2530	–	–
037.7-06.0	[WC4]	–	–	–	–	–	–
048.7+01.9	[WC4]	85	0.91±0.45	9.18±1.54	321±143	3.11±0.44	2
060.4+01.5	[WC11]	110	8.96±3.9	–	–	–	–
061.4-09.5	[WO2]	89	0.29±0.11	0.94±0.15	126±51	2.98±0.42	11
064.7+05.0	[WC9]	111	3.66±1.5	5.4±0.9	4884±1960	6.75±0.95	1
068.3-02.7	[WC9]	97	13.0±8.5	8.8±1.4	8835±5770	14.5±2.05	–
089.0+00.3	[WO3]	78	1.47±0.63	4.75±0.94	336±137	2.00±0.28	9
089.8-05.1	[WR]	124	2.08±0.95	5.9±1.1	4816±2127	5.22±0.74	9
093.9-00.1	[WC11]	132	2.11±1.12	–	6687±3536	–	–
094.0+27.4	[WO]	–	–	–	–	–	12+
096.3+02.3	[WC4-6]	80	1.39±0.6	2.6±0.42	361±153	2.15±0.3	10
118.0-08.6	[WC]	89	0.76±0.31	3.9±0.63	335±138	1.60±0.23	5
118.8-74.7	WC OVI	70	0.10±0.05	–	13±7.0	–	12
120.0+09.8	[WC8]	101	0.68±0.28	1.1±0.2	564±226	3.74±0.53	–
130.2+01.3	[WO4]	79	0.92±0.41	3.4±0.52	223±102	1.40±0.2	7
144.5+06.5	[WO4]	75	0.32±0.15	1.53±0.25	60±26	1.17±0.16	3
146.7+07.6	[WC11]	136	0.68±0.28	0.78±0.12	2516±1042	9.68±1.37	–
189.1+19.8	[WO1]	87	0.39±0.17	1.1±0.2	155±64	2.70±0.39	–
189.8+07.7	WC-OVI	63	5.59±2.4	18.3±3.6	439±184	3.67±0.52	8
216.0+07.4	[WC4]	62	1.10±0.48	–	80±34	–	–
222.8-04.2	[WC7-8]	103	0.35±0.19	–	321±178	–	–
243.3-01.0	[WO1]	90	0.58±0.23	2.6±0.4	272±109	3.2±0.45	10

PNG	class	T_d (K)	M_d ($10^{-4}M_\odot$)	m_d/m_g (10^{-3})	L_{IR} (L_\odot)	IRE	Exc. class
270.1-02.9	[WC5-7]	101	0.69±0.28	1.2±0.21	565±226	3.75±0.53	-
272.8+01.0	[WC9-10]	-	-	-	-	-	-
278.1-05.9	[WO2]	94	0.60±0.24	0.91±0.14	347±139	1.54±0.22	8
278.8+04.9	[WO1]	104	0.81±0.35	2.45±0.4	774±329	6.85±0.97	-
285.4+01.5	[WO4]	114	1.49±0.55	3.17±0.51	2270±1250	5.08±0.70	3
284.2-05.3	[WO3]	-	-	-	-	-	-
286.3+02.8	[WO3]	97	0.22±0.11	0.71±0.12	149±72	6.94±0.98	12
291.3+08.4	[WO4]-[WC4]	73	-	7.08±1.41	1161.21	-	-
291.3-26.2	[WC10]	-	-	-	-	-	-
292.4+04.1	[WC5-6]	85	2.53±1.0	8.7±1.4	887±358	5.19±0.73	2
297.0+06.5	[WO2]	-	-	-	-	-	-
300.7-02.0	[WC4]	104	2.66±1.2	4.15±0.56	2558±1106	2.72±0.45	4
302.0-01.6	[WC9]	-	-	-	-	-	-
306.4-00.6	[W03]pec	84	0.34±0.15	1.06±0.2	114±48	1.78±0.25	-
307.2-03.4	[WO1]	77	0.26±0.1	0.41±0.07	57±22	1.21±0.17	10
308.5+02.5	[WC4]	-	-	-	-	-	-
309.0-04.2 ²	[WC9]	91	0.88±0.36	3.7±0.62	435±176	8.04±1.13	3
309.1-04.3	[WO4]	94	2.44±1.0	14±2.4	1422±584	3.53±0.5	3
309.8-01.6	[WC4]	-	-	-	-	-	-
313.9+02.8	[WC9]	82	-	-	-	-	-
319.6+15.7	[WR]	63	2.2±0.92	3.7±0.68	135±54	1.47±0.21	5
321.0+03.9	[WC10]	120	39.0±16	44.8±7.7	9700±5300	>25.00	1
324.0+03.5	[WO4]pec	-	-	-	-	-	-
327.5-02.2	[WR]	-	-	-	-	-	-
327.1-02.2	[WC9]	126	1.11±0.53	19.6±3.5	2767±1298	6.83±0.97	1
332.9-09.9	[WC10]	107	-	-	-	-	-
336.2-06.9	[WO4]	-	-	-	-	-	3
336.5+05.5	[WO4]	-	-	-	-	-	-
337.4+01.6	[WC9]	99	-	-	-	-	1
341.5+12.1	[WC3]	63	-	-	-	-	-
348.4+04.9	[WC10]	108	0.37±0.16	-	431±176	-	-
350.1-03.9	[WC4-5]	82	0.63±0.29	25.4±4.4	184±85	7.01±0.98	9
350.9+04.4	[WC11]	124	0.75±0.32	1.1±0.2	1728±737	4.40±0.62	1
351.5-06.5	[WO2]	73	3.23±1.3	-	530±219	-	-
352.9+11.4	[WC11]	106	5.3±2.2	-	5618±2336	-	-
355.4-04.0	[WO2]	89	0.47±0.2	1.9±0.3	206±87	7.30±1.0	11
355.2-02.5	[WC4]	-	-	-	-	-	3
355.9+03.6	[WC11]	215	0.11±0.06	-	4165±1936	-	-
355.9-04.4	[WO3]	-	-	-	-	-	-
356.0-04.2	[WO2-3]	-	-	-	-	-	-
356.1+02.7	[WC5-6]	146	0.92±0.5	-	4811±2604	-	-
356.8-03.6	[WC11]	-	-	-	-	-	-
357.1-04.7	[WC11]	102	7.20±3.4	21±4	6263±2926	17.37±2.45	1
357.3+03.3	[WC11]	92	0.78±0.33	-	405±168	-	-
357.4-03.2	[WO2-3]	-	-	-	-	-	7
358.3-21.6	[WO3]	81	0.89±0.37	2.3±0.4	245±100	1.36±0.19	9
359.8+03.5	[WC4]	-	-	-	-	-	-
359.9-04.5	[WC4]	99	1.66±0.61	2.42±0.41	1247±730	2.85±0.42	3
359.8+05.6 ¹	[WC11]	104	1.15±0.5	6.7±1.2	1109±472	6.08±0.85	1

¹ Escudero & Costa (2001); ² Garcia-Rojas, Pena, Morriset et al. (2012); ³ Phillips (2005); ⁴ Escudero, Costa & Macial (2004)

⁵ Balick, Perinotto, Maccioni et al. (1994); ⁶ Bohigas (2003); ⁷ Kwitter & Henry (2001); ⁸ Madsen, Frew & Parker (2006);

⁹ Perinotto & Corradi (1998)

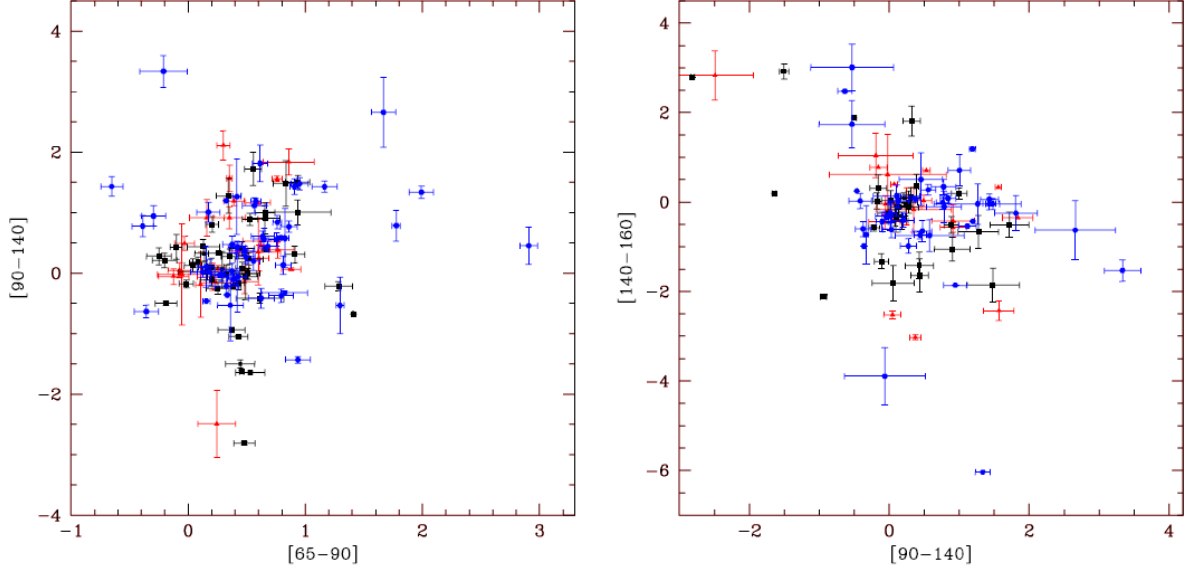


Figure 4. Far-IR colour-colour diagrams of PNe using *Akari* measurements. Data description as given in Fig. 1. See the text for details.

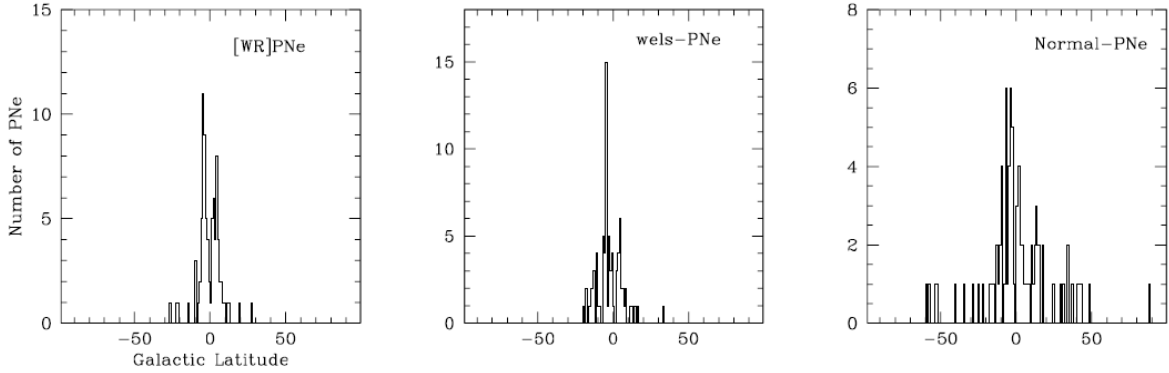


Figure 5. Histograms showing Galactic distribution of [WR] PNe, *wels*-PNe and normal PNe. See the text for details.

4 GAS AND DUST PROPERTIES

The properties of gas and dust components of [WR] PNe, *wels*-PNe and normal-PNe were derived using IRAS photometric data and are given in Table 2, Table 3 and in Table 4 respectively. In this section we discuss these properties in more details.

4.1 Dust Colour Temperature

The colour temperature of thermal equilibrium dust in a PN can be derived using its continuum fluxes at *IRAS* 25- and $60\mu\text{m}$ bands. Though there is a distribution of dust temperature

Table 3. Nebular parameters derived for *wels*-PNe (see the text for details)

PNG	T_d (K)	M_d ($10^{-4}M_{\odot}$)	m_d/m_g (10^{-3})	L_{IR} (L_{\odot})	IRE	Exc. class
000.4+04.4 ¹	82	1.84±0.89	–	539±258	–	–
000.7-02.7	–	–	–	–	–	8
000.7+04.7	95	3.32±1.8	8.89±1.5	2032±1098	5.10±0.72	2
000.9-02.0	–	–	–	–	–	3
001.7-04.6	93	1.34±0.57	4.8±0.83	735±304	3.58±0.5	5
002.0-06.2	90	1.60±0.67	–	749±305	–	–
002.0-13.4	116	0.55±0.23	4.7±0.82	921±373	3.18±0.45	1
002.6+08.1	81	2.26±1.0	18.8±3.2	623±270	4.86±0.69	3
003.2-04.4	–	–	–	–	–	3
003.7-04.6	84	1.62±0.68	1.17±0.2	537±323	3.72±0.55	9
003.9-14.9	127	0.37±0.15	1.04±0.19	972±390	2.55±0.36	–
004.2-04.3	–	–	–	–	–	3
004.6+06.0	77	2.45±1.1	20±3.6	525±229	4.63±0.66	1
006.4+02.0	100	2.38±1.0	4.4±0.74	1882±775	3.95±0.56	2
007.0-06.8	94	2.22±0.93	3.2±0.57	1287±520	3.44±0.49	2
007.8-04.4	85	2.85±1.2	32±5.5	1002±412	5.73±0.81	–
008.1-04.7	81	2.51±1.1	–	3451±1590	5.70±0.71	2
009.6-10.6	80	1.58±0.61	–	410±241	4.96±0.7	8
010.8-01.8	78	2.78±1.2	11.9±2.28	636±263	2.55±0.36	3
011.7-00.6	70	5.16±2.3	–	686±309	–	–
012.5-09.8	–	–	–	–	–	6
013.7-10.6	81	–	–	–	–	6
014.2+03.8	97	–	–	–	–	–
014.4-06.1 ¹	75	2.28±1.1	–	428±220	–	–
014.3-05.5	–	–	–	–	–	–
016.4-01.9	91	1.34±0.76	11±2.0	662±369	5.03±0.71	11
019.4-05.3	114	3.2±1.4	6.1±1.0	4872±2107	5.15±0.73	3
025.8-17.9	94	0.49±0.2	0.8±0.13	284±113	1.73±0.25	10
034.6+11.8	120	0.77±0.33	1.2±0.22	1530±622	2.57±0.36	2
038.2+12.0	110	1.05±0.52	2.0±0.35	1342±654	3.51±0.49	1
046.4-04.1	94	1.81±0.78	1.01±0.17	1052±446	2.3±0.34	5
051.9-03.8	92	1.49±0.65	9.3±1.5	777±335	4.54±0.64	6
054.1-12.1	89	1.01±0.42	4.3±0.7	445±175	1.78±0.25	2
055.5-00.5	114	0.75±0.35	2.44±0.44	1143±511	4.93±0.70	2
057.2-08.9	84	1.29±0.55	5.4±0.90	427±118	1.83±0.26	5
058.3-10.9	144	0.6±0.28	1.0±0.2	2953±1343	2.09±0.3	6
068.7+14.8	–	–	–	–	–	2
081.2-14.9 ³	–	–	–	–	–	12
096.4+29.9	93	1.28±0.57	4.8±0.8	707±304	–	7
159.0-15.1	90	0.56±0.30	0.51±0.11	266±152	1.61±0.21	10
190.3-17.7	85	0.63±0.25	1.0±0.17	222±87	1.36±0.19	4
194.2+02.5	106	0.65±0.28	1.3±0.2	690±286	2.10±0.29	9
208.5+33.2	79	1.03±0.40	≥ 30±14	2503±1001	–	–
221.0-01.4	–	–	–	–	–	–
221.3-12.3	106	0.4±0.17	0.69±0.12	421±170	1.17±0.17	10
253.9+05.7	90	1.74±0.73	6.2±1.1	812±332	3.7±0.52	4
258.1-00.3	115	0.41±0.18	0.79±0.1	663±279	1.83±0.26	3
264.4-12.7	109	0.35±0.15	1.1±0.2	431±176	1.34±0.19	2
274.6+02.1	94	1.02±0.45	4.4±0.7	590±259	2.39±0.34	3
289.8+07.7	–	–	–	–	–	10

PNG	T_d (K)	M_d ($10^{-4}M_\odot$)	m_d/m_g (10^{-3})	L_{IR} (L_\odot)	IRE	Exc. class
315.1-13.0	117	1.27±0.535	11.9±2.0	2212±908	5.26±0.74	10
316.1+08.4	84	2.16±0.88	22.7±3.5	714±289	7.1±1.0	10
329.9+03.7	78	-	-	-	-	-
331.3+16.8	108	0.23±0.09	1.2±0.2	267±107	1.3±0.19	10
331.8-02.3	-	-	-	-	-	-
333.4-04.3	79	0.83±0.37	-	203±110	-	-
341.8+05.4	78	2.78±1.2	11.9±2.3	633±263	2.29±0.6	8
343.9-05.8 ¹	-	-	-	-	-	10
351.7-06.6 ¹	-	-	-	-	-	3
355.9-04.2	86	3.15±1.5	10.5±2.3	1172±516	4.1±0.57	1
356.2-04.4	105	1.32±0.56	3.42±0.6	1338±548	2.15±0.3	7
356.7-04.8	82	0.8±0.33	7.1±1.1	234±96	1.94±0.27	9
356.9+04.4	89	9.90±4.5	35.12±4.71	4375±1899	8.58±1.2	7
357.1+03.6	-	-	-	-	-	2
357.2-04.5	100	0.68±0.3	0.62±0.11	529±285	1.72±0.21	3
358.0-04.6	-	-	-	-	-	-
358.9+03.3	97	3.71±1.6	1.3±0.2	2523±1065	4.71±0.67	-

in a PN due different radial distances of grains from the heating central star and also due to the grain size distribution, the resulting IR spectrum from a PN reasonably indicates a characteristic dust temperature of the PN (Stasinska & Szczerba 1999). We derived the characteristic dust colour temperatures, or simply the colour temperatures (T_d) of PNe using their *IRAS* 25- and $60\mu\text{m}$ fluxes. The ratio of fluxes emitted from dust at wavelengths λ_1 and λ_2 in the optically thin limit is:

$$F_{\lambda_1}/F_{\lambda_2} = (\lambda_2/\lambda_1)^\alpha \times B_{\lambda_1}(T_d)/B_{\lambda_2}(T_d) \quad (2)$$

where, $B_{\lambda_1}(T_d)$ and $B_{\lambda_2}(T_d)$ are the values of Planckian function at λ_1 and λ_2 for T_d . We fitted the *IRAS* fluxes using this function with an emissivity index $\alpha = 1$ to obtain T_d . The dust colour temperatures were computed for PNe if their *IRAS* 25- and $60\mu\text{m}$ fluxes are available with error estimates. The assumed value of α is typical for micron-sized grains. The colour temperatures for PNe were earlier derived by Zhang & Kwok (1993) using *IRAS* fluxes with a blackbody model ($\alpha = 0$) fit. However, dust do not emit like blackbodies and as discussed earlier, a modified black body curve with $\alpha = 1$ represents the continuum emission from circumstellar dust better. Increasing the value of α will result a lower colour temperature for dust. The error in dust colour temperature is due to the errors in the *IRAS* fluxes for a given α . This error was examined by fitting the curve to extreme ranges in the flux ratios. The error in T_d estimation never exceeded 10% and we have kept this as the error in T_d estimation. The mean dust colour temperatures of [WR] PNe, *wels*-PNe and of normal-PNe were derived and are found to be quite similar taking their respective dispersions (or the observed ranges) into account (see Table 5).

Table 4. Nebular parameters derived for normal PNe (see the text for details)

PNG	T_d (K)	M_d ($10^{-4}M_{\odot}$)	m_d/m_g (10^{-3})	L_{IR} (L_{\odot})	IRE	Exc. class
000.1+17.2	98	2.25±1.15	5.0±0.8	1609±816	4.29±0.61	1
002.2-02.7	240	0.58±0.29	0.42±0.09	3691±1692	11.6±1.64	3
002.4-03.7	105	1.38±0.62	11.1±2.1	1392±612	5.23±0.74	-
002.7-52.4	-	-	-	-	-	2
008.2+06.8 ⁴	147	1.06±0.56	2.7±0.47	5771±3001	13.7±1.9	1
010.8+18.0	95	-	-	-	-	-
010.7-06.4	143	0.31±0.13	0.40±0.72	1459±580	1.71±0.24	5
011.7-06.6	-	-	-	-	-	-
014.6-04.3	87	2.35±0.90	3.7±0.68	925±376	2.45±0.35	7
015.9+03.3	100	-	-	-	-	1
017.3-21.9	-	-	-	-	-	1
017.6-10.2	81	0.29±0.12	25.3±6.7	80±32	7.83±1.11	12
025.3+40.8	98	0.88±0.32	-	632±217	-	6
025.4-04.7	75	0.70±0.2	4.6±0.77	13.22±5.2	0.82±0.11	10
027.6-09.6	106	0.81±0.33	1.1±0.2	863±344	1.62±0.22	4
034.5-06.7	59	3.74±1.5	4.1±0.7	212±85	1.62±0.23	9
035.9-01.1	81	0.10±0.06	-	24±13	0.93±0.13	3
036.1-57.1	-	-	-	-	-	2
037.7-34.5 ⁵	86	1.32±0.55	5.2±1	491±198	1.92±0.27	7
042.9-06.9	166	0.25±0.10	1.6±0.27	2474±996	4.33±0.61	3
043.1+37.7	90	1.17±0.48	2.29±0.38	548±219	2.17±0.3	4
045.4-02.7	132	2.23±1.02	15.5±2.7	7087±3152	45.9±6.5	3
045.7-04.5	88	0.37±0.16	7.9±1.4	153±63	3.1±0.44	12
047.0+42.4	-	-	-	-	-	-
049.4+02.4	62	0.75±0.34	-	54±24	29.9±4.2	1
051.0+02.8	132	-	-	-	-	3
053.8-03.0	-	-	-	-	-	1
055.4+16.0	-	-	-	-	-	2
060.1-07.7	94	1.56±0.64	5.75±0.9	903±365	2.1±0.29	11
060.8-03.6	63	0.05±0.02	-	4±2	-	11
061.0+08.0	95	0.24±0.10	7.1±1.1	147±61	4.1±0.57	12+
063.1+13.9	65	1.03±0.42	1.3±0.2	95±38	1.45±0.21	10
064.6+48.2	76	0.48±0.19	17.8±2.8	96±38	3.30±0.47	11
072.7-17.1	-	-	-	-	-	-
077.6+14.7	-	-	-	-	-	3
082.5+11.3	-	-	-	-	-	1
083.5+12.7	93	0.67±0.07	1.97±0.3	368±14.9	2.1±0.29	8
089.3-02.2	101	1.41±0.61	-	1175±611	11.7±2.1	-
093.4+05.4	83	0.47±0.2	17.8±0.39	146±59	4.26±0.6	11
095.2+00.7	127	1.08±0.52	1.0±0.2	2827±1361	2.45±0.35	3
102.9-02.3 ⁶	-	-	-	-	-	3
107.8+02.3	89	0.64±0.27	5.1±0.83	284±118	2.13±0.3	9
114.0-04.6	-	-	-	-	-	-
123.6+34.5	93	0.46±0.05	4.3±0.71	254±15	2.23±0.32	3
147.4-02.3	95	0.68±0.29	2.9±0.46	414±175	0.79±0.11	3
148.4+57.0 ⁷	-	-	-	-	-	8
165.5-06.5	93	-	-	-	-	3
165.5-15.2	58	0.17±0.07	-	9±4	-	-
166.1+10.4	104	0.60±0.24	1.2±0.2	574±230	1.73±0.25	-
167.4-09.1	115	0.26±0.11	1.2±0.2	408±170	1.74±0.25	1

PNG	T_d (K)	M_d ($10^{-4}M_\odot$)	m_d/m_g (10^{-3})	L_{IR} (L_\odot)	IRE	Exc. class
170.3+15.8	100	0.11±0.05	–	84±35	–	12+
193.6-09.5	–	–	–	–	–	8
196.6-10.9	101	0.38±0.16	0.8±0.13	316±127	3.52±0.5	12
197.8-03.3	–	–	–	–	–	–
197.8+17.3	78	0.48±0.02	1.1±0.2	110±45	1.27±0.18	8
204.1+04.7	–	–	–	–	–	1
206.4-40.5	83	1.6±0.5	–	500±265	1.45±0.20	8
214.9+07.8	94	0.04±0.02	2.0±0.4	25±10	1.13±0.16	12
215.2-24.2	124	0.67±0.28	1.8±0.3	1553±637	2.49±0.35	1
215.6+03.6	59	0.67±0.34	2.8±0.5	38±18	1.57±0.22	9
219.1+31.2 ⁸	–	–	–	–	–	1
220.3-53.9	71	–	–	–	–	12
231.8+04.1	63	0.42±0.19	0.7±0.2	33±13	1.1±0.15	5
233.5-16.3	90	0.13±0.06	7.6±1.2	61±28	3.36±0.47	12+
234.9-01.4	109	0.37±0.17	0.75±0.2	456±271	1.57±0.24	1
238.0+34.8	–	–	–	–	–	1
239.6+13.9	98	0.10±0.04	3.2±0.6	67±27	2.17±0.3	12
241.0+02.3	–	–	–	–	–	11
242.6-11.6	69	0.63±0.26	1.4±0.2	79±32	0.74±0.1	3
245.4+01.6	64	2.95±1.3	4.1±0.7	251±105	3.01±0.4	9
248.7+29.5	–	–	–	–	–	–
253.5+10.7	105	0.03±0.01	–	25±13	–	12
255.3-59.6	–	–	–	–	–	–
261.0+32.0	87	0.50±0.27	–	197±105	–	9
261.9+08.5	78	0.13±0.04	5.0±0.9	30±12	1.07±0.15	10
263.2+00.4	–	–	–	–	–	1
272.1+12.3	59	1.67±0.5	–	94±43	–	5
277.1-03.8	70	0.19±0.07	0.38±0.06	25±10	1.15±0.16	11
279.6-03.1 ⁹	90	0.38±0.15	3.4±0.5	176±71	1.48±0.2	10
283.6+25.3	–	–	–	–	–	1
285.7-14.9	89	0.32±0.13	3.6±0.96	144±68	1.50±0.2	10
294.1+14.4	–	–	–	–	–	3
294.1+43.6	98	0.07±0.03	–	49±20	–	12+
327.8+10.0	88	1.65±0.7	16.8±2.8	691±276	2.52±0.36	6
341.6+13.7	76	0.23±0.1	1.1±0.2	47±19	0.20±0.03	11
345.4+00.1	–	–	–	–	–	3
303.6+40.0	–	–	–	–	–	1
305.1+01.4	139	–	–	–	–	1
308.6-12.2	–	–	–	–	–	1
339.9+88.4	–	–	–	–	–	–
310.3+24.7	–	–	–	–	–	12
318.4+41.4	–	–	–	–	–	–
320.1-09.6	102	3.71±1.4	2.8±0.8	3245±1880	9.30±1.5	–
320.3-28.8	102	0.45±0.13	1.5±0.5	391±203	2.00±0.3	3
325.8-12.8	171	0.15±0.07	1.1±0.2	1963±823	9.28±1.1	1
331.4-03.5	–	–	–	–	–	1
336.3-05.6	100	0.40±0.12	–	319±153	2.06±0.32	9
345.5+15.1	–	–	–	–	–	–
349.5+01.0	76	4.67±0.2	17.8±2.8	937±379	4.04±0.65	10
357.6+01.7	–	–	–	–	–	3

A plot between the dust colour temperatures of PNe and their ages will be an useful tool to see if there is a change in dust temperature as a PN evolves. A robust, distance-independent parameter to indicate the age of a PN is the nebular $H\beta$ surface brightness ($S_{H\beta}$; Stasinska & Szczerba 1999; Gorny & Tylenda 2000). $S_{H\beta}$ decreases as a PN ages. If

the interstellar reddening corrected nebular $H\beta$ flux is $F_{H\beta}$ and the angular radius of the optical nebula is θ then $S_{H\beta}$ is defined as:

$$S_{H\beta} = F_{H\beta}/\pi\theta^2 \quad (3)$$

PNe are often non-spherical in shape. The values of θ for all PNe in our sample are calculated from their angular sizes of major and minor axes given in FPB16, by equating the area. We could not estimate the error in $S_{H\beta}$ as the errors in angular extends of optical nebulae are not available; however, it is unlikely that the error in $S_{H\beta}$ will be significant enough to change the trends seen in our analysis. Fig 7a shows the plot of T_d against $S_{H\beta}$ for [WR] PNe, *wels*-PNe and in normal PNe, indicating that the dust colour temperature decreases steadily with age for PNe. This is similar to the earlier finding by Gorny et al. (2001) for [WR] and non-[WR] PNe and also by Pottasch et al. (1984). However, we resolve [WR] PNe, *wels*-PNe and normal-PNe in our dust colour temperature plot against age. To quantitatively find the strength of correlation between T_d and $S_{H\beta}$, we estimate the Pearson correlation coefficient with an associated probability (r, p) for the three groups of PNe and they are also shown in the figure. The values of (r, p) indicates that the correlation of T_d with age is quite tight for all the three groups of PNe. Fig 6a can be understood in terms of expansion of the PN which dilutes the stellar radiation field inside the nebula and as a result of this the grains are less heated. The figure also shows that [WR] PNe and *wels*-PNe are not observed at large ages like normal PNe. [WR] PNe are not observed below $S_{H\beta} = 3 \times 10^{-4}$ and *wels*-PNe are seen only above $S_{H\beta} = 10^{-3}$, however about 20% of normal PNe are seen with lower $S_{H\beta}$ values, down to 2×10^{-5} . This may show that [WR] PNe and *wels*-PNe are relatively younger than a good fraction of normal PNe. The highest values of $S_{H\beta}$ for *wels*-PNe and normal PNe are same while one [WR]PN (Hen 2-113; [WC10]) shows a value which is ~ 2.5 times more than this. The minimum dust temperature observed for [WR] PNe is 63K and for normal PNe it is 59K whereas *wels*-PNe show a significantly higher value of 77.

Fig 6b shows a plot of T_d vs $S_{H\beta}$ for different subtypes of [WR] PNe; viz. [WCE] ([WO1] to [WC4]), [WCL] ([WC9] to [WC11]) (See AN03) and the intermediate ones, [WCg], ([WC5] to [WC8]). The figure brings out a trend of decrease in T_d from [WCE] to [WCg] to [WCL]. Together, there is also a continuity in the plot, whereas in Fig 6a each group of PNe shows such a continuity.

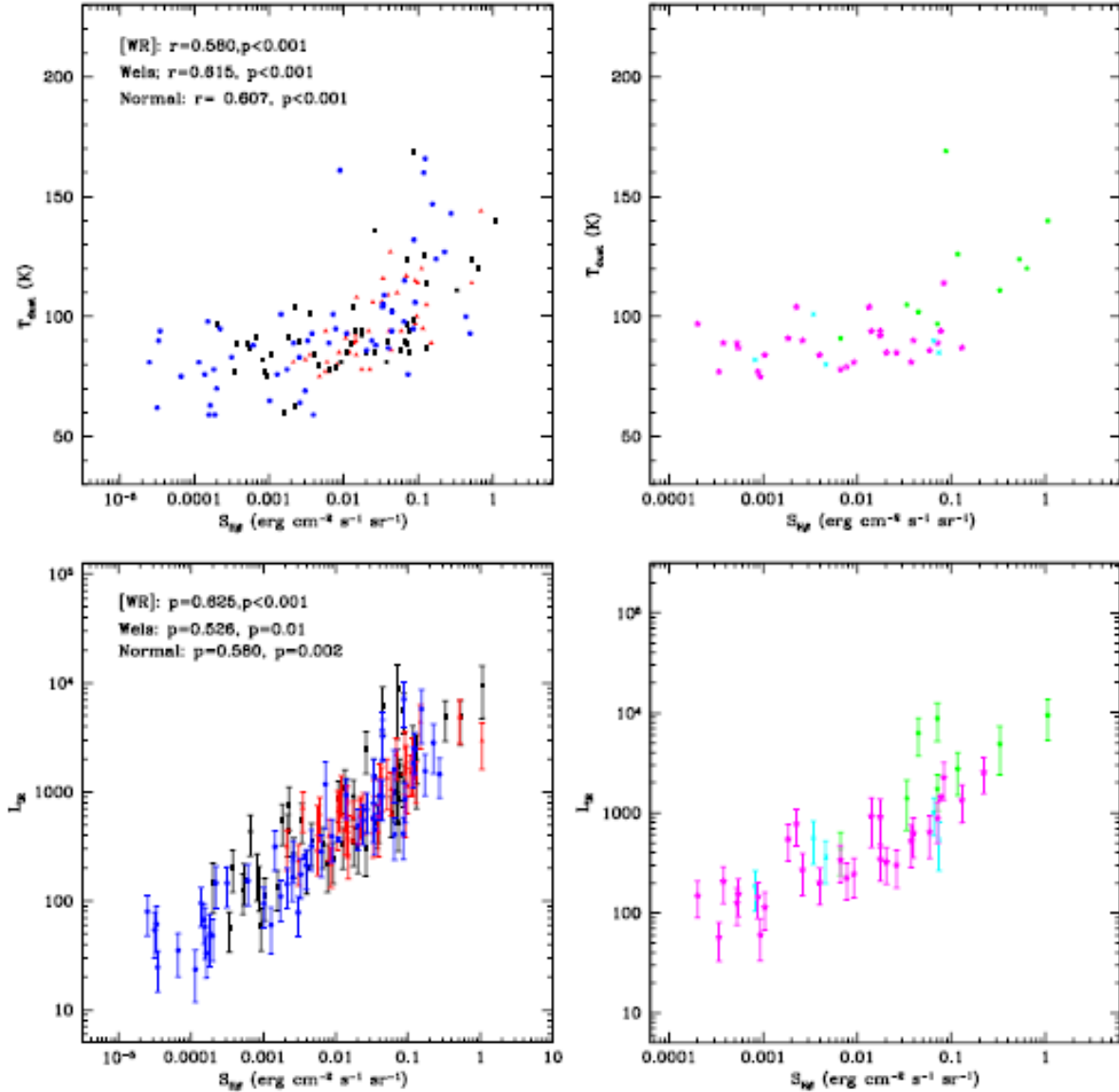


Figure 6. *Top:* a) Dust colour temperature is plotted against $S_{H\beta}$ for [WR] PNe, *wels*-PNe and normal PNe (left) and b) for the subtypes of [WR] PNe (right). *Bottom:* c) IR luminosity for [WR] PNe, *wels*-PNe and normal PNe (left); d) IR luminosity for the subtypes of [WR] PNe (right). Data description as shown in Fig 1. See the text for details.

4.2 IR luminosity and IR excess

We estimate the IR luminosity (L_{IR}) of a PN as the total IR continuum energy emitted by thermal equilibrium dust. Hence L_{IR} does not include the emission due to dust features and the emission due to the hot dust component. L_{IR} of a PN is calculated using its *IRAS* fluxes at 25- and $60\mu\text{m}$ bands. We fitted a modified blackbody flux distribution function with an emissivity index $\alpha = 1$, and integrated the whole curve to get L_{IR} . Error in L_{IR} was estimated from the error in the integrated flux and from (and dominated by) the error in distance measurement which is given in FPB16. The IR excess (IRE) represents the excess

amount of L_{IR} in terms of what can be accounted by absorption of $Ly\alpha$ radiation produced in the nebula. The IRE of a PN was calculated from its L_{IR} and its reddening corrected nebular $H\beta$ flux using the relation given in Stasinska & Szczerba (1999; equation 6). The error in IRE was estimated from the errors in respective parameters used to calculate IRE. A plot on the variation of L_{IR} and IRE of PNe against their $S_{H\beta}$ will be useful to address how these parameters change as the PN evolves. Fig 6c shows the variation of L_{IR} with $S_{H\beta}$ for [WR] PNe, *wels*-PNe and normal-PNe along with their respective (r, p) values showing the correlation strengths. The figure displays a tight correlation between L_{IR} with $S_{H\beta}$ for all the three groups of PNe, implying that L_{IR} decreases strongly with nebular age for all PNe. The variation of L_{IR} with $S_{H\beta}$ for the subgroups of [WR] PNe can be seen in Fig 6d which shows a decrease in L_{IR} for PNe with late type to early type [WR] central stars. However, as seen in Fig 7a, IRE is not correlated with $S_{H\beta}$ for all the PNe, which was also found earlier by Stasinska & Szczerba (1999) for their sample. This is in contrast with the suggestion given by Pottasch et al. (1984) who had studied L_{IR} and IRE of PNe and proposed that younger PNe have higher IRE. As a PN expands to a larger size and the central star is becoming hotter, its L_{IR} drops steadily keeping the IRE constant.

The average values and dispersions of L_{IR} and IRE for the three groups of PNe were computed and are compared in Table 5. As it can be seen in the table, the average value of L_{IR} for [WR] PNe, *wels*-PNe and normal PNe are very similar. However, the mean values of IRE for the three groups of PNe show that *wels*-PNe and normal PNe have quite similar values, while [WR] PNe show a tendency towards a larger mean value. Among [WR] PNe He 2-113, M 2-43, He 2-459, IRAS 21282+5050, He 1-43, SwST 1, K 2-16, BD+30 3639 and IC 5117 show very large values for L_{IR} (IRE) than the other candidates in the group. Their respective values are $9700L_{\odot}$ (≥ 25), $9498L_{\odot}$ (7.5), $8834L_{\odot}$ (14.5), $6689L_{\odot}$ (-), $6226L_{\odot}$ (17), $5824L_{\odot}$ (15), $5618L_{\odot}$ (-), $4884L_{\odot}$ (6.75), $4816L_{\odot}$ (5.2) and $4165L_{\odot}$ (-). All of them belong to the [WCL] subtype. M 1-61 and M 3-38 are the two *wels*-PNe which show large L_{IR} (IRE); their values are $4877L_{\odot}$ (5.1) and $4375L_{\odot}$ (8.5). Two normal PNe, namely Vy 2-2 and He 2-260 have their respective L_{IR} (IRE) of $7087L_{\odot}$ (15) and $5771L_{\odot}$ (13). The lowest L_{IR} in our sample was seen for a few normal PNe. From the equation used to compute IRE (equation 6. in Stasinska & Szczerba 1999), a weak correlation between IRE and $S_{H\beta}$ for all PNe implies that L_{IR} decreases with the nebular $H\beta$ flux for a PN as it expands.

4.3 Dust mass and dust-to-gas mass ratio

The dust masses and the dust-to-gas mass ratios of PNe are also examined in order to understand the nature of the three groups of PNe considered in this study. For an optically thin dust cloud, a criterion which is readily fulfilled in and above the mid-IR region for the thermal grains of PNe, the total dust mass can be obtained from the continuum flux observed at one band where the dust emission dominates. If m_d is the total dust mass of a PN, it is calculated from the dust temperature and flux at an IR band in the optically thin limit using the following relation (Stasinska & Szczerba 1999):

$$m_d = F_\nu(\lambda)D^2/Q_{abs,\nu}B_\nu(T_d) \quad (4)$$

where, D is the distance to the nebula, $F_\nu(\lambda)$ is the flux at an IR band (we have taken the flux at *IRAS* $60\mu\text{m}$ which is least contaminated by atomic emission) and $B_\nu(T_d)$ is the Planckian function at frequency ν (corresponding to $60\mu\text{m}$) for a dust colour temperature of T_d . $Q_{abs,\nu}(\lambda)$ is the dust absorption coefficient at λ , which has a value of $74 \text{ cm}^2\text{g}^{-1}$ at $60\mu\text{m}$. The error in m_d was estimated from the errors in respective parameters used to derive m_d and is dominated by the error in distance.

Dust masses were estimated for all PNe for which *IRAS* $60\mu\text{m}$ fluxes are available with error measurements. Fig 7b shows the plot of dust mass against $S_{H\beta}$ for [WR] PNe, *wels*-PNe and normal-PNe along with their respective (r, p) values. The figure brings out that the dust mass of a PN is weakly correlated with its age. It shows that the dust is neither destroyed nor significantly reduced as a PN evolves, for all the three PNe groups. The mean dust mass values arrived for the [WR] PNe, *wels*-PNe and normal PNe are given in Table 5 along with their dispersions. [WR] PNe (and also *wels*-PNe) have a tendency towards larger mean dust mass in compared to the normal PNe. It may imply that dust can be created more efficiently by the progenitors of [WR] PNe and *wels*-PNe in compared to the progenitors of normal-PNe. Large IRE for [WR] PNe can also be produced when their dust masses are also high. The lowest m_d in our sample was seen for a few normal PNe.

The dust-to-gas mass ratios (m_d/m_g) of PNe were calculated using their *IRAS* fluxes at 25- and $60\mu\text{m}$ bands. Reddening-corrected nebular $H\beta$ fluxes and the nebular electron temperatures and densities which are required for estimating m_d/m_g were taken from the literature. We used the relation given by Stasinska & Szczerba (1999; equation 5). The dust temperatures required for this calculation were obtained earlier in Section 4.1. Error in

m_d/m_g was estimated from the errors in the respective parameters used to derive m_d/m_g . The derived values of m_d/m_g are plotted against $S_{H\beta}$ for the three groups of PNe in Fig 7b and their (r, p) values are shown. As it can be seen in the figure, m_d/m_g is not correlated with the age of the nebula, as also was noted by Gorny et al. (2001). These observed trends imply that dust destruction is inefficient as a PN evolves. In contrast, Pottasch et al. (1984) suggested from a sample of 46 PNe that m_d/m_g decreases with nebular radius and hence with nebular age.

The mean values of m_d/m_g were estimated for [WR] PNe, *wels*-PNe and normal-PNe which are shown in Table 5 along with their dispersions. All the three groups of PNe show similar mean values, taking the dispersion into account. Gorny et al. (2001) also have suggested that there is no significant difference in m_d/m_g for [WR] PNe and non-[WR] PNe. As the mean dust mass tends to have a larger value for [WR] PNe (and *wels*-PNe), similar values of mean m_d/m_g for all the three group of PNe possibly shows that [WR] PNe (and *wels*-PNe) have proportionally larger mean gas mass than normal-PNe. The mean electron densities (n_e) for [WR] PNe, *wels*-PNe normal-PNe are also similar (Table 5).

The chemical nature of the grain (amorphous carbon or amorphous silicate) in PN can also contribute to the estimation of T_d , m_d , m_d/m_g , L_{IR} and IRE. To derive the nebular and dust parameters above we have considered a dust emissivity index of $\alpha = 1$ and $Q_{abs,\nu}(\lambda) = 74.38$ (Stasinska & Szczerba 1999), which are more suitable for amorphous carbon grains. If the grain type is chosen to be amorphous silicate then $\alpha \sim 2$ and $Q_{abs,\nu}(\lambda) = 53.45$ (Stasinska & Szczerba 1999); which will result about 30% difference in the derived values of T_d , m_d and m_d/m_g and a few percent decrease in the L_{IR} and IRE. The mean nebular and dust parameters for the three groups of PNe taking the grains to be amorphous silicates are also given in Table 5 along with their respective values derived for amorphous carbon grains. As noted by Stasinska & Szczerba (1999), m_d/m_g can be overestimated for PNe that are not fully ionized, however, such cases should represent a small fraction for the low surface brightness PNe.

Szczerba et al. (2001) noted from their IR spectroscopic study of 16 [WR] PNe that $\sim 75\%$ of them show the signatures of PAH emission and hence they can have carbon based dust. We have searched *Spitzer* IRS spectra for the sample of PNe considered in our study. We found that 18 [WR]PNe, 15 *wels*-PNe and 19 normal PNe have their spectra in the *Spitzer Heritage Archive*. We also looked at the *ISO – SWS* spectra where, the 3.3- and 4.6 μ features are either absent or very weak. Our preliminary inspection of *Spitzer* IRS

spectra shows that 16 [WR]PNe (88%) and 10 *wels*-PNe (67%) and 10 normal PNe (52%) in our sample show clear presence of PAH features. However, [WR]PNe usually show stronger PAH features than the other two groups, confirming the trend seen in our photometric study in Section 3.2 that they likely to have brighter $12\mu\text{m}$ *IRAS* band. These spectra also show that the dust chemistry in most [WR]PNe and *wels*-PNe are carbon-rich. Gorny et al. (2001) argued from their *IRAS* CCDMs of carbon stars and [WR] PNe that they are evolutionarily connected. The distribution of nebular C/O ratio of [WR] PNe is similar with the other PNe as found by Gorny & Stansinska (1995). However, many of the *wels* appear in Mendez (1991) are oxygen rich stars and are related to variable stars with oxygen-rich circumstellar shells (Acker, Gorny & Cuisinier 1996). The grain chemistry is not known for many of the PNe in our sample.

Excitation class of a PN is an important parameter which represents the nebular spectral class. It is related to several parameters of the PN like the nebular structure, mass, chemical compositions and the temperature and luminosity of its central star as discussed by Gurzadyan & Egikyan (1991). Using the relations given by them to derive the excitation classes of PNe, we attempt to see if there are differences in the distributions of spectral classes of [WR] PNe, *wels*-PNe and normal PNe. We have determined the excitation classes (from 1 to 3) using the line fluxes of [OIII] (at 4959 \AA and at 5007 \AA) and $\text{H}\beta$ and higher excitation classes (from 4 to 12) were derived from the line fluxes of [OIII] and He II (at 4686 \AA). Though, the ionic emission line fluxes for most PNe were from Acker, Ochsenbein, Stenholm et al. (1992), for some PNe they are taken from other published results (see the references listed in Table 2). In Fig 8 we show the histograms of excitation classes for 54 [WR] PNe, 55 *wels*-PNe and 84 normal-PNe. A two sample Kolmogorov-Smirnov test was performed between the distributions of excitation classes for different groups of PNe to see if they are similar. The value of the test statistics between the distributions of [WR] PNe and *wels*-PNe is $D = 0.067$ and the probability to find the test statistics below the critical value is $P = 0.99$. This shows that the data sample of excitation classes of [WR] PNe and *wels*-PNe come from similar distribution. A Kolmogorov-Smirnov test performed between the distributions of [WR] PNe and normal-PNe shows $D = 0.21, P = 0.89$ and between *wels*-PNe and normal PNe shows the values of $D = 0.267, P = 0.70$. Hence, the excitation class distribution of normal PNe is different from that of the [WR] PNe and *wels*-PNe. The emission line flux ratios of [OIII] to $\text{H}\beta$ are similar (smaller than 15) for all PNe except A 30 (ratio = 40, has a *wels* central star), A 78 (ratio = 33 in the inner knot; Jacoby 1983; has a

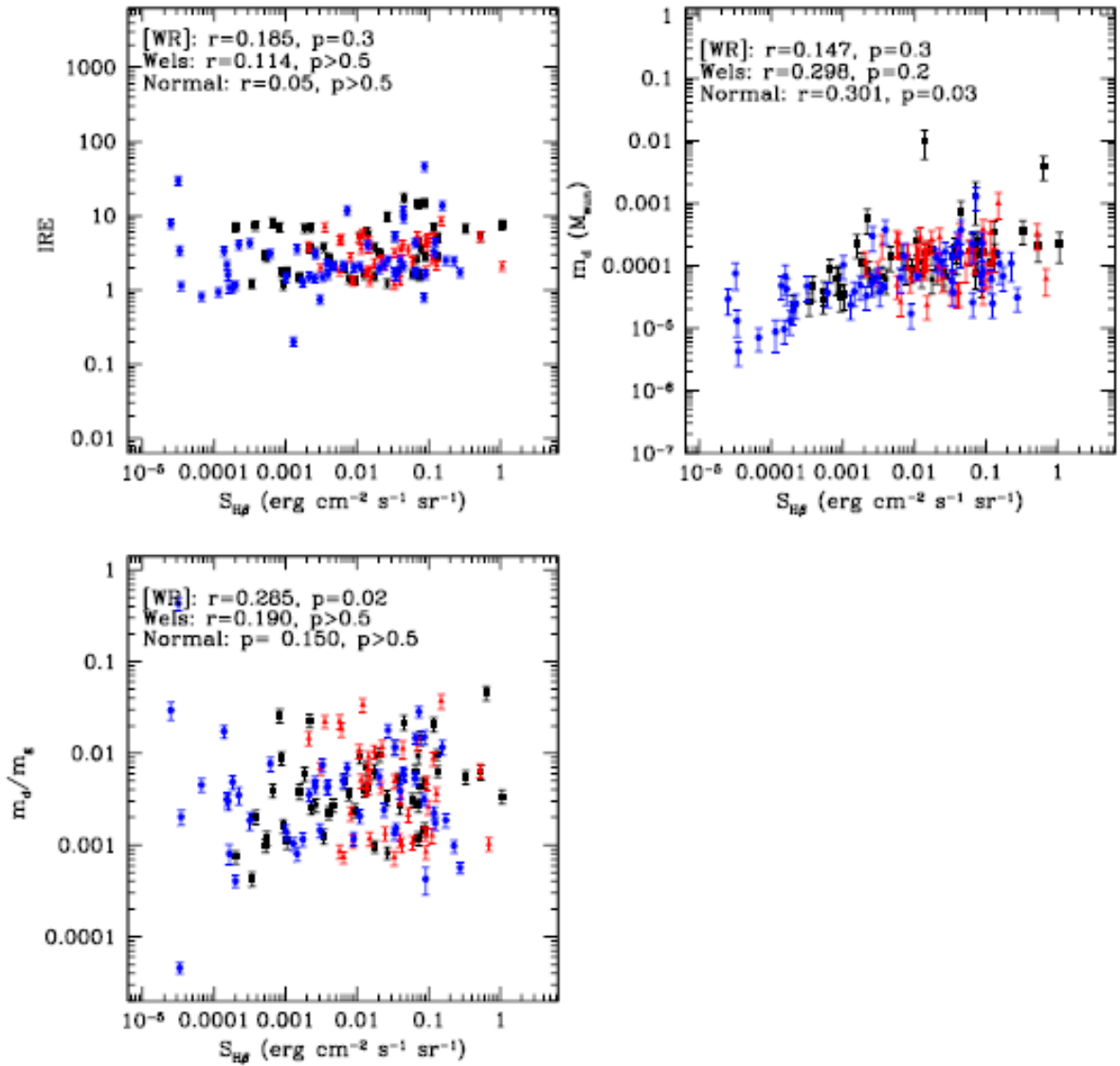


Figure 7. The dust parameters of [WR] PNe, *wels*-PNe and normal PNe plotted against $S_{H\beta}$. a) IRE (top left); b) m_{dust} (top right); c) m_d/m_g (bottom left). Data description as given in Fig. 1. See the text for details.

wels central star) and IRAS 15154-5258 (ratio = 74 for the central region, Harrington 1996; has a [WR] central star). The large ratio of [OIII] to H β fluxes implies that dust heating could be significant in the nebula (Harrington 1996). Another PN which shows a large ratio (ratio = 102) is IRAS 18333-2357 (Gillett et al. 1989; Muthumariappan, Parthasarathy & Ita 2013), however, its central star identification as a H-poor star is uncertain.

4.4 Very small dust grains

The excess emission over the thermal equilibrium dust emission from a PN in the 1-15 μ m region should arise from very small grain population (VSG). These grains thermally fluctuate by absorbing UV photons from the hot CSPN and attain high temperatures (~ 1000 K) then they cool down by emitting at longer wavelengths. VSG emit significantly in the near-IR to the N band. The presence of VSG has been seen in circumstellar environments, for example, in PNe A30 (Borkowski et al. 1994) and IRAS 18333-2357 (Muthumariappan, Parthasarathy & Ita 2013). As seen in Section 3.1, larger fraction of [WR] PNe, in compared to other groups, are distributed close to the dust line in the near-IR CCDM ('ND' region in Fig 1) where the VSG contribute significantly. This hot dust component would come from the winds of the [WR] central stars (Gorny et al. 2001), similar to that was suggested for the near-IR colours of the population I WC stars (Williams et al. 1987). A good fraction of *wels*-PNe also show this hot dust emission. However, the average values of *WISE* [3.4-4.6] colours for the three groups of PNe are very close, taking their dispersions into account (see Table 1).

Table 5. Mean values of the parameters of [WR] PNe, *wels*-PNe and normal PNe along with their dispersion. The number of candidates were given in brackets.

Parameter (mean value)	[WR] PNe (No. of PNe)	<i>wels</i> -PNe (No. of PNe)	normal PNe (No. of PNe)
$T_d(K)$	96 ± 25 (78)	95 ± 14 (52)	93 ± 31 (67)
	75 ± 13	75 ± 9	74 ± 17
$\log[m_d(M_\odot)]$	-3.83 ± 0.52 (70)	-3.86 ± 0.35 (49)	-4.33 ± 0.56 (61)
	-3.57 ± 0.51	-3.59 ± 0.35	-4.06 ± 0.56
$\log[m_d/m_g]$	-2.38 ± 0.63 (52)	-2.37 ± 0.50 (43)	-2.51 ± 0.58 (48)
	-2.19 ± 0.60	-2.17 ± 0.50	-2.30 ± 0.57
$\log[n_e(cm^{-3})]$	3.54 ± 0.46 (45)	3.63 ± 0.41 (29)	3.52 ± 0.54 (31)
$\log[L_{IR}(L_\odot)]$	2.91 ± 0.55 (67)	2.90 ± 0.32 (49)	2.76 ± 0.50 (61)
	2.88 ± 0.53	2.88 ± 0.32	2.72 ± 0.47
$\log[IRE]$	0.64 ± 0.60 (54)	0.47 ± 0.22 (42)	0.43 ± 0.40 (52)
	0.62 ± 0.58	0.45 ± 0.22	0.42 ± 0.40

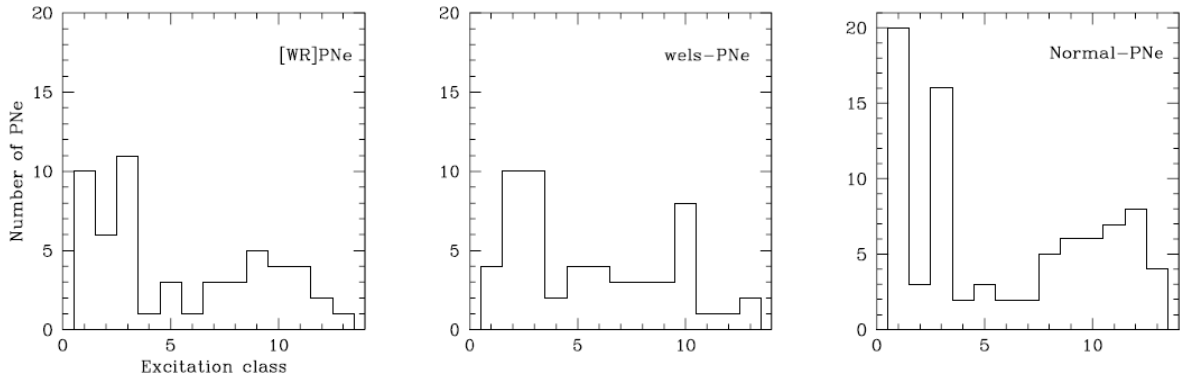


Figure 8. Histograms of excitation classes of [WR] PNe, *wels*-PNe and normal PNe. See the text for details.

5 DISCUSSION

We discuss here using our results and those available in the literature if there is a possibility for evolutionary sequences between different groups of PNe considered in this study.

5.1 Evolutionary Sequence between the subtypes of [WR] PNe

AN03 showed that the central star temperatures of [WR] PNe, derived from energy-balance method, increase along the [WC] to [WO] evolutionary sequence. Gorny et al. (2000) plotted $S_{H\beta}$ of the subtypes of [WR] PNe against their central star spectral types which showed a steady decrease in nebular $S_{H\beta}$ for PNe with central star types from [WCL] to [WCE]. Our dust colour temperature plot against $S_{H\beta}$ for the subtypes of [WR] PNe in Fig 6b shows that the PNe with [WCL] central stars occupy the region with higher values of $S_{H\beta}$ and T_d while the PNe with [WCE] stars are seen in the region where they have lower values (though they show good overlap in the intermediate values) and the plot shows a continuity. Further, there

is no significant difference in the distribution of PNe with [WCL] and [WCE] central stars in the 'NS' and 'ND' regions of the near-IR CCDM shown in Fig 1b. The figure also shows that there is no [WCL] PN in the nebular box. This may imply that nebular emission becomes more significant as [WR]PNe evolve. Hence this study supports the proposal given earlier by AN03 and Girard, Koppen & Acker (2007) that [WCL] and [WCE] are evolutionarily connected. However, it should be noted that all the well studied PNe with [WCL] central stars show dual dust chemistry which is not commonly observed in PNe with [WCE] central stars (De Marco 2008).

5.2 Is there a Evolutionary Sequence between [WR] PNe and *wels*-PNe ?

From their stellar terminal velocity *vs* effective temperature diagram, AN03 suggested that the [WR] sample shows a mean central star mass that is higher than the value shown by normal CSPNe. However, on the age-temperature diagram, Gesicki et al. (2006) found that *wels* are located on tracks of both high and low stellar mass while [WR] stars take a range of intermediate masses. They also find that nebular turbulence is almost universal for [WR] PNe and commonly observed for *wels*-PNe but it is quite rare for normal PNe. They suggested that one group of *wels* may have an evolutionary connection with the [WO] stars as the photospheric temperature increases, otherwise [WR] and *wels* appear to represent independent evolutionary tracks. Girard, Koppen & Acker (2007) found from their analysis of chemical compositions of a sample of [WR] PNe and *wels*-PNe that *wels*-PNe evidently belong to a separate subclass of PNe, and unlikely they have evolutionary connection with [WR] PNe.

From Fig 6a and Fig 6c we find that the distribution of dust colour temperatures and IR luminosities for [WR] PNe, *wels*-PNe and normal PNe against $S_{H\beta}$ are continuous for each group. In other words, removing one group of PNe do not make the plots discontinuous, suggesting that they don't form an evolutionary sequence. The Galactic latitudinal distribution and the excitation class distribution of [WR] PNe and *wels*-PNe are quite similar and they are distinctly different from that of the normal PNe. This reaffirms that these three groups of PNe make three PNe populations and also indicates that [WR] PNe, *wels*-PNe do not form an evolutionarily sequence. The mean values of m_d are similar for [WR] PNe and *wels*-PNe whereas normal-PNe have a tendency towards a lower mean value for mean

m_d . These observed similarities show some underlying common features between [WR] PNe and *wels*-PNe, which are not owned by normal ones, which may be related to their origin. Hence, our study supports the proposal that [WR] PNe, *wels*-PNe and normal PNe are not evolutionarily connected but in some way [WR] PNe and *wels*-PNe are related. However, the 2MASS CCDM shows that the distribution of [WR] PNe is somewhat different from that of *wels*-PNe. [WR] PNe commonly show strong IR emission features but *wels*-PNe show the weakest emission. The dispersions shown by *wels*-PNe in the mean values of parameters given in Table 1 and Table 5 are narrower than their respective dispersions shown by other two groups suggesting that they are relatively homogeneous.

A handful of PNe show H-poor ejections which are located inside their (older) H-rich outer shells. Among five such PNe, four of them have their central stars classified. Two PNe (A30 and A78) have *wels* central stars and other two (A58 and IRAS 15154-5258), which are relatively younger, have [WR] central stars. The values of m_d and L_{IR} of two of these H-poor PNe are quite high: they are $1.08 \times 10^{-3} M_{\odot}$ and $4780 L_{\odot}$ for A58 and $1.02 \times 10^{-3} M_{\odot}$ and $2502 L_{\odot}$ for A30. *IRAS* measurements for A78 are not available and hence these values were not calculated. Zijlstra (2001) suggested an evolutionary sequence of A58 \rightarrow IRAS 15154-5258 \rightarrow A30/A78 and argued the weaker winds in A30/A78 could be due to their declining luminosity. Though our study argues that [WR] PNe and *wels*-PNe do not form an evolutionary sequence, it requires still more work to be done addressing all the related findings to reach a final conclusion.

6 CONCLUSIONS

The main conclusions of the paper are the following:

1) In the near-IR CCDM, [WR] PNe are usually seen away from the nebular box whereas, *wels*-PNe are commonly seen inside the nebular box. [WR] PNe have more tendency of finding them towards the dust line when compared to other PNe.

2) [WR] PNe show a tendency towards brighter *IRAS* 12 μ m band in compared to *wels*-PNe and normal PNe, which possibly show that they have strong PAH emission.

3) Cool AGB dust in PNe traced by *IRAS* 25- and 60 μ m bands have very similar colour

for all the three groups of PNe.

4) All PNe show a tight correlation of decrease in T_d with nebular age. *wels*-PNe are not seen at dust temperature lower than 77K whereas normal PNe have dust temperature as low as 59K. Minimum $H\beta$ surface brightness seen for [WR] PNe and *wels*-PNe are significantly larger than the value shown by normal-PNe, implying that they are relatively younger. While L_{IR} of PNe are strongly correlated (decrease) with their age, m_d and m_d/m_g do not change noticeably as the PN evolves.

5) [WR] PNe and *wels*-PNe are relatively distributed closer to the Galactic plane in compared to the normal PNe. The excitation class distributions of [WR] PNe is quite similar to that of *wels*-PNe and both have significant deviation from the distribution shown by normal PNe.

7 ACKNOWLEDGEMENTS

This research has made use of the SIMBAD database, operated at CDS, Strasbourg, France. This publication makes use of data products from the Two Micron All Sky Survey, which is a joint project of the University of Massachusetts and the Infrared Processing and Analysis Centre, funded by the National Aeronautics and Space Administration and the National Science Foundation. This work is based in part on observations made with *WISE*, obtained from the NASA/IPAC Infrared Science Archive, operated by the Jet Propulsion Laboratory, California Institute of Technology, under contract with the National Aeronautics and Space Administration. The authors thank the referee for his/her comments and suggestions.

REFERENCES

- Acker A., Ochsenbein F. & Stenholm B. et al. 1992, Strasbourg-ESO Catalogue of Galactic Planetary Nebulae, European Southern Observatory, Garching
- Acker A., Neiner C. 2003, A&A, 403, 659
- Balick B., Perinotto M., Maccioni A., Terzian Y., & Hajian A. 1994, ApJ, 424, 800
- Bohigas J. 2003, RMxAA, 39, 149
- Borkowski K.J., Harrington J.P., 1991, ApJ, 379, 168
- Borkowski K.J., Sarazin C.L., Soker N., 1990, ApJ, 360, 173

- Crowther P.A. 2008, in Werner K., & Rauch T., eds., ASP Conf. Series, Vol 391, 'Hydrogen Deficient stars. Astron. Soc. Pac Conf. Series., San Francisco, p. 83
- Crowther P.A., De Marco, O. & Barlow M.J. 1998, MNRAS, 296, 367
- Cutri R.M. et al., 2003, 2MASS All-Sky Catalog of point sources. The IRSA 2MASS All-Sky Point Source Catalog, Tech. Rep., IPAC, Caltech. <http://irsa.ipac.caltech.edu/applications/Gator/>
- De Marco O. in Werner K., & Rauch T., eds., ASP Conf. Series, Vol 391, 'Hydrogen Deficient stars. Astron. Soc. Pac Conf. Series., San Francisco, p. 208
- Escudero A.V., & Costa R.D.D, 2001, A&A, 380, 300
- Escudero A.V., Costa R.D.D & Macial W.J. 2004, A&A, 414, 211
- Frew D.J., Parker Q.A., & Bojicic I.S. 2016, MNRAS, 455, 1459
- Garcia-Rojas J., Pena M., Morriset C., Mesa-Delgado A., & Ruiz M.T. 2012, A&A 538, A54
- Gesicky K., Zijlstra A.A., Acker A. et al. 2006, A&A, 451, 925
- Gillet F.C., Jacoby G.H., Joyce R.R., Cohen J.G., Neugebauer G., Soifer B.T., Nakajima T., Mathews K., 1989, ApJ, 338, 862
- Girard P., Koppen J. & Acker A. 2007, A&A, 463, 265
- Gorny S. K. & Stansinska G. 1995, A&A, 303, 893
- Gorny S.K. Tylanda R. 2000, A&A, 362, 1008
- Gorny S.K., Stasinska G., Szczerba R. et al. 2001, A&A, 377, 1007
- Gurzadyan G.A. & Egikyan A.G. 1991, ApSS, 175, 15
- Hajduk M., Zijlstra A.A., Gesicky K. 2010, MNRAS, 406, 626
- Ishihara D. et al., 2010, A&A, 514, A1
- Kingsburgh R.L. & Barlow M.J. 1994, MNRAS, 271, 257
- Kwitter K. B. & Henry R. B. C. 2001, ApJ, 562, 804
- Leuenhagen U., & Hamann W.R. & Jeffrey C.S. 1996, A&A, 312, 167
- Koorneef J. 1983, A&AS, 51, 489
- Madsen G. J., Frew D. J., Parker Q. A., Reynolds R. J., Haffner L. M., 2006, in Barlow M.J., & Mendez, R.H. eds., IAU Symp. 234, 'Planetary Nebulae in our Galaxy and Beyond' p. 455
- Mendez R. 1999, IAUS, 145, 375
- Muthumariappan C., Kwok S. & Volk V. 2006, ApJ, 640, 353
- Muthumariappan C., Parthasarathy M. & Ita Y. 2013, MNRAS, 435, 606
- Nagebauer G. Habing H.J., Van Duinen R. et al., 1984, ApJ, 278, L1
- Phillips J.P. 2005, MNRAS, 361, 283
- Parthasarathy M., Acker A. & Stenholm B. 1998, A&A, 329, L9
- Parthasarathy M. 1999., in Le Betre T., Lebre A. & Waelkens C., eds., IAU Symp. 191, 'Asymptotic Giant Branch Stars' p. 474
- Persi P., Preite-Martinez A., Ferrari-Toniolo M. & Spinoglio L. 1987, IAU Symp. 122, 499
- Perinotto M. & Corradi R.L.M. 1998, A&A, 332, 721
- Plets H., Waelkens C., Oudmaijes R.D. et al. 1997, A&A, 323, 513
- Pottasch S. R. et al. 1984 A&A, 138, 10
- Schonberner D., Ballick B. & Jacob R. 2018, A&A, 609, A126
- Shirahata M., Matsuura S., Hasegawa S. et al. 2009, PASJ, 61, 737
- Stanghellini L., Bucciarelli B., Lattanzi M.G. et al. 2019, ApJ (in press)
- Stasinska G., Szczerba R. 1999, A&A, 352, 297
- Siebenmorgen R., Krügel E., Mathis J.S., 1992, A&A, 266, 501
- Szczerba R., Gorny S.K., Stasinska G. et al. 2001, ApSS, 275, 113
- Tielens A.G.G.M., 2008, ARA&A, 46, 289

- Todt H., Grafener G. & Hamann W.-R. 2006, in Barlow M.J., Mendez R.H. eds., Proc. IAU Symp. 234, Planetary Nebulae in our Galaxy and Beyond, Cambridge Univ. Press, Cambridge, p. 127
- Tylenda R. & Gorny S.K. 1993, Acta Astron. 43, 389
- Whitelock P.A. 1985, MNRAS, 213, 56
- Weidmann W.A. & Gamen R. 2011, A&A, 526, A6
- Weidmann W.A., Mendez R.H & Gamen R. 2015, A&A, 579, 86
- Williams P.M., van der Hucht K.A. & Te P.S. 1987, A&A, 182, 91
- Werner K., Herwig F. 2006, PASP, 118, 183
- Wright E.L. et al., 2010, AJ, 140, 1868
- Yerra B.K., Reddy B.E., Muthumariappan C., Zhao G. 2015, A&A, 577, 10
- Zhang C.Y. & Kwok S. 1993, ApJS, 88, 137
- Zijlstra A.A., 2002, Ap&SS, 279, 171